

Article

Design of Fiber-Composite/Metal–Hybrid Structures Made by Multi-Stage Coreless Filament Winding

Pascal Mindermann ^{1,*}, Ralf Müllner ^{2,3}, Erik Dieringer ^{2,3}, Christof Ocker ⁴, René Klink ⁴,
Markus Merkel ⁴ and Götz T. Gresser ^{1,5,*}

- ¹ Institute for Textile and Fiber Technologies, University of Stuttgart, Pfaffenwaldring 9, 70569 Stuttgart, Germany
- ² Institute of Industrial Manufacturing and Management, University of Stuttgart, Allmandring 35, 70569 Stuttgart, Germany; ralf.muellner@ipa.fraunhofer.de (R.M.); erik.dieringer@ipa.fraunhofer.de (E.D.)
- ³ Fraunhofer Institute for Manufacturing Engineering and Automation, Nobelstraße 12, 70569 Stuttgart, Germany
- ⁴ Institute for Virtual Product Development, Aalen University of Applied Sciences, Beethovenstraße 1, 73430 Aalen, Germany; christof.ocker@hs-aalen.de (C.O.); rene.klink@hs-aalen.de (R.K.); markus.merkel@hs-aalen.de (M.M.)
- ⁵ German Institutes of Textile and Fiber Research Denkendorf, Körschtalstraße 26, 73770 Denkendorf, Germany
- * Correspondence: pascal.mindermann@itft.uni-stuttgart.de (P.M.); goetz.gresser@itf.de (G.T.G.)



Citation: Mindermann, P.; Müllner, R.; Dieringer, E.; Ocker, C.; Klink, R.; Merkel, M.; Gresser, G.T. Design of Fiber-Composite/Metal–Hybrid Structures Made by Multi-Stage Coreless Filament Winding. *Appl. Sci.* **2022**, *12*, 2296. <https://doi.org/10.3390/app12052296>

Academic Editors: Stelios K. Georgantzinou, Georgios I. Giannopoulos, Konstantinos Stamoulis and Stylianos Markolefas

Received: 5 February 2022
Accepted: 20 February 2022
Published: 22 February 2022

Publisher's Note: MDPI stays neutral with regard to jurisdictional claims in published maps and institutional affiliations.



Copyright: © 2022 by the authors. Licensee MDPI, Basel, Switzerland. This article is an open access article distributed under the terms and conditions of the Creative Commons Attribution (CC BY) license (<https://creativecommons.org/licenses/by/4.0/>).

Featured Application: The methods presented in this study assist in fabricating load-bearing structures with high mass-specific mechanical performance at various scales. Possible applications include primary and secondary structures in engineering, architecture, automotive, or aerospace industries.

Abstract: Additive manufacturing processes, such as coreless filament winding with fiber composites or laser powder bed fusion with metals, can produce lightweight structures while exhibiting process-specific characteristics. Those features must be accounted for to successfully combine multiple processes and materials. This hybrid approach can merge the different benefits to realize mass savings in load-bearing structures with high mass-specific stiffnesses, strict geometrical tolerances, and machinability. In this study, a digital tool for coreless filament winding was developed to support all project phases by natively capturing the process-specific characteristics. As a demonstration, an aluminum base plate was stiffened by a coreless wound fiber-composite structure, which was attached by additively manufactured metallic winding pins. The geometrical deviations and surface roughness of the pins were investigated to describe the interface. The concept of multi-stage winding was introduced to reduce fiber–fiber interaction. The demonstration example exhibited an increase in mass-specific component stiffness by a factor of 2.5 with only 1/5 of the mass of a state-of-the-art reference. The hybrid design approach holds great potential to increase performance if process-specific features, interfaces, material interaction, and processes interdependencies are aligned during the digitized design phase.

Keywords: coreless filament winding; multi-stage winding; laser powder bed fusion; fiber-composite/metal–hybrid structure; digital design tool; graph theory

1. Introduction

Beginning in the 1960s, the adoption of carbon fiber reinforced plastics (CFRPs) in structural engineering was primarily motivated by their superior mass-specific mechanical parameters, which can be tailored to the individual application [1]. While CFRPs incorporate a low thermal expansion [2] together with non-magnetic [3] and non-corrosive properties [4], their drawbacks include limited recyclability [5], reparability [6], and often non-destructive quality control [7], as well as a high environmental impact [8].

Coreless filament winding (CFW) is an emerging composite manufacturing process that has not yet reached its full potential for high-performing and efficient structures due to limiting software design tools. In CFW [9–12], a roving is spanned freely between point-like anchors to additively manufacture a component, such as lattices [13,14] or shells [15,16]. The constantly tensioned [17] fiber strand is usually impregnated online [18] with a thermoset resin in a bath or by an end-effector [19]. Alternatively, pre-tows [20] can be deployed. CFW is distinguished from conventional winding techniques [21,22] in that the component shape can be well described by straight lines connecting several anchor points in a specific sequence. Geometrical deviations in the fiber net can arise through fiber–fiber interaction only, whereas in hybrid forms [23,24], the fibers are also partially supported by surfaces. The benefit of CFW is decoupling the tooling from the composite structure, which enables cost-effective adaptability of components and leads to minimizing tooling costs while increasing fiber–fiber interaction, which is hard to predict and control. Recent demonstrations of CFW were directed towards building applications [25] and validated design [26], simulation [27], manufacturing [28], testing [29], approval, and monitoring [30] procedures. Where these research-orientated custom solutions are fragmented between different software tools and platforms, widely used proprietary CAD/CAM tools are intended for prismatic geometries in isotropic materials. Software directed towards composite and textile-based characteristics mostly depends on a layer-based design [31], which CFW often does not exhibit. Recently, a first step towards an integrative software tool for CFW was undertaken by the creation of a common data framework, which was validated in a case study [20,32].

One challenge of designing with CFW is to find the structurally most efficient framework structure in compliance with CFW fabrication characteristics. This is driven by two effects: minor reconfigurations of the fiber net can cause disproportional changes [33] in the mechanical behavior of the structure, and the addition of an additional node exponentially increases the number of possible configurations. The number of all configurations is given by $n^{(n-2)}$ depending on the number of nodes n [34]. Although this includes self-similar configurations and ones that do not involve all given nodes, the number is still so large that evaluating all reasonable combinations is currently not economical for technical applications. Another challenge in CFW is the digital capturing of fabrication deviations to feed structural simulations. Due to the geometrical complexity, fiber–resin-, and fiber–fiber interactions, current simulation tools can resolve only simpler components (Figure 1) on the roving level [35]. Larger and more complex structures are calculated based on approximative models, which rely on a correct calibration of material properties, which are generated by full-scale destructive tests [36].

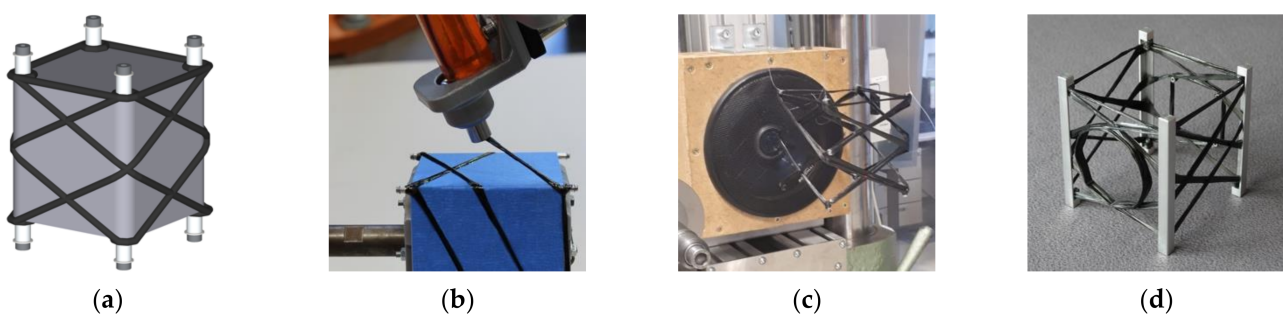


Figure 1. Process flow of coreless filament winding. (a) Digital representation of the CFW object during the design phase; (b) Robotic manufacturing of the fiber composite by hybrid CFW; (c) Eigenfrequency testing of the load-bearing fiber-composite structure; (d) Final component after assembly.

During the design process, less sophisticated structural simulations are sufficient to evaluate fiber net configurations, but the rather linear design process [33] (Figure 1) is still limited by human intuition and experience. In multi-material [37] components, the various materials can take on different tasks, and material parameters can be set depending on the location.

Unlike CFW, additive manufacturing (AM), in the form of 3D printing, has evolved in the last decades, from being used in prototyping and research to industrial manufacturing. One reason for this is the presence of the complete digital process chain from design to machine control in AM. A variety of AM processes, for thermoplastic, short-/long-fiber-reinforced plastics, and metals enables the user to create complex shapes that are not possible or not economical with conventional manufacturing technologies, such as lathing, milling, and drilling. Similar to CFW, in AM, specific parameters become relevant, such as layer-interphases, supports and infills, wall thicknesses, warping, sagging, build plate adhesion, overhangs, and multi-material phenomenon. AM also decouples the component design from the manufacturing tool, which allows each component to be individual. Although CFW is restricted to having similar component topologies within the same fabrication setup, it outperforms AM in build volume and speed [19]. In this study, laser powder bed fusion (LPBF) was utilized to manufacture the anchor elements for the CFW structure. In LPBF, a moveable laser beam selectively melts metal powder layer-by-layer together under an inert atmosphere [38].

Conventional manufacturing technologies remain a valid option for manifold applications, especially when AM or CFW do not match the needed design language, are too slow in manufacturing, exhibit too high material costs, or lack other features. A combination of AM with the subsequent use of conventional technologies is possible but not advisable in CFW due to the fiber-composite character of the structures.

This study presents methods to synergistically combine CFW, AM, and conventional manufacturing methods, and to exploit the specific characteristics of each process and material system. Within an application-based case study, this design approach was showcased, together with a custom-coded CFW design and data management tool that accompanied all project phases. The selected case study object offered a direct comparison with the state of the art in mechanical engineering. The digital tool aims to improve the CFW design workflow by utilizing graph-theoretical representations to streamline manufacturing by providing a digitally verified winding plan and to facilitate object management through database capabilities. A holistic digital representation can increase the process efficiency and manageability, resulting in overall cost savings. The implementation of multi-stage winding [39] into CFW aims to reduce the deformation of the fiber net caused by fiber–fiber interactions, which simplifies digitally representing the object. Manufacturing characteristics of the used LPBF processes were investigated with relevance to the design approach and fiber-composite material. In particular, the dimensional accuracy of the winding anchors must be ensured for the multi-material interplay.

2. Materials and Methods

2.1. Object-Oriented Design and Management Tool

This study developed a digital CFW design tool to assist during all the project phases. CFW structures are best described by a graph-theoretical [40] approach due to their shape characteristics. In the most fundamental level of detail, anchors are represented by nodes as points with cartesian coordinates, and edges as connecting lines represent the fiber bundles (Figure 2b). The undirected graph is stored as an edge list, not as an adjacency matrix [41]. This is more efficient because only a few of all possible connections are present. Self-connections (1–1, 2–2, . . .) are not relevant; therefore, the diagonal of the adjacency matrix is filled with zeros. Nodes are numbered with integers and may contain data on external force inductions and the anchor orientation, both as vectors (Figure 2a). The fiber path (Figure 2c) is stored as a sequence of nodes, which is called winding syntax [42]. It is often separated into several sub-syntaxes, which start and end at the same node. It can be advantageous to define the path as a repetition of local direction statements if the syntax has a regular shape.

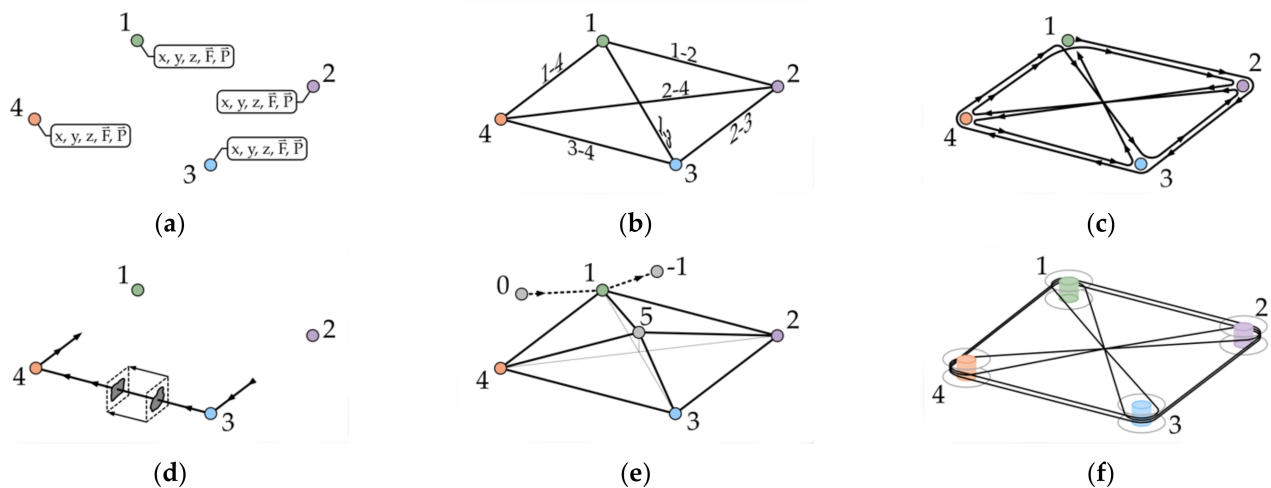


Figure 2. Digital representation of different levels of detail of the same winding object. (a) Point cloud of the nodes, containing information on the cartesian coordinates, external forces, and the anchor orientation; (b) Graph of the winding object; (c) Winding path as sequence of nodes [1, 2, 3, 4, 1, 3, 2, 4, 3, 1]; (d) Local information (e.g., cross-section) defined along the path; (e) Control point 5 at the crossing point deforms the fiber net, points 0 and -1 position the fiber ends; 2–5–4 and 1–5–3 are sections, 1–5, 2–5, 3–5, and 4–5 are segments; (f) Nodes are represented as sleeve–washer combinations with the winding path in a discretized form.

Building upon this fundamental digital representation (node coordinates, graph, and path), several features can be implemented independently from each other to increase the level of detail and the precision of predictions:

1. Additional control points can be implemented to connect two fibers at a crossing point properly, to deform the fiber net, or both (point 5, see Figure 2e). Nodes represent anchors, while control points do not. A single edge between two nodes or control points is called a segment, while the connection between two nodes is called a section and may contain several segments.
2. Two additional nodes ($0 = \text{pre_start_node}$, $-1 = \text{post_end_node}$, see Table A1) represent the protruding segments required at the beginning and end of the CFW process (Figure 2e). The model can be adjusted to match the fabricated structure by relocating existing nodes or control points and by adding new ones.
3. A (uniform) subdivision of the segments along the fiber path can be implemented to add local information along the fiber path, such as cross-sectional parameters (Figure 2d), local fiber volume ratio (FVR) deviations, or strain-field measurements by a fiber-optical sensor (FOS) system [43].
4. Around anchors, the actual circular fiber arrangement caused by the wrapping can be implemented with a polyline (Figure 2f). Depending on the hooking condition [44], the fiber path is longer than the direct connection, and the ends of the adjacent segments are radially offset. This lets the actual fiber net deviate from the graph for structures that are small in relation to their anchors.

The developed digital design tool (Figure 3) is an object-oriented Python (version 3.7.7) script to digitally represent and analyze CFW objects. It has dependencies mainly to numpy [45], pandas [46], plotly [47], and scipy [48]. The script operates on all beforementioned levels of detail and helps during all project phases, from design, over simulation, and fabrication to managing the finished components. When adding a level of detail, the fundamental representation of the object is preserved.

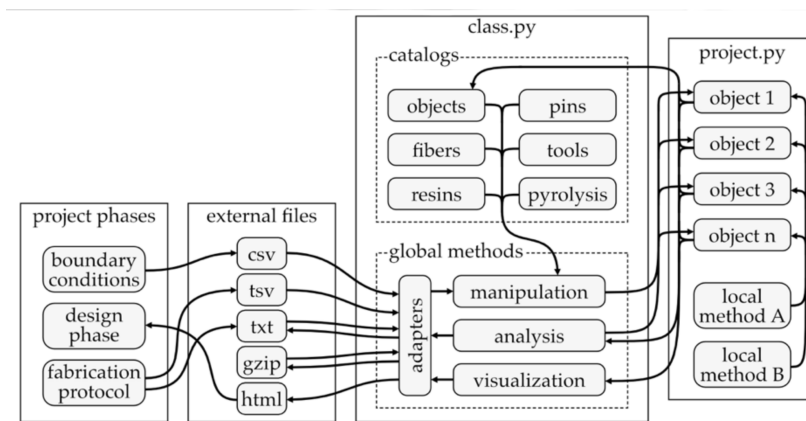


Figure 3. Domains of the CFW design and management tool. Multiple project files are possible.

The tool consists of a class containing predefined functions (methods) and catalogs that permanently store object-independent parameters. One or more project files store the attributes of the winding objects and access the catalogs and methods of the class. If necessary, further custom methods can also be defined locally in the project files. Methods are used to manipulate, analyze, and visualize data. Adaptor methods provide import, export, and cache functionalities. External csv files provide data of nodes, control points, and the graph. During the design phase, dynamic visualizations and tables are output as html. The gzip format is used to cache data between calculation steps. The syntax can be exported as txt for winding preparation. After production and mechanical testing, the measurement data and syntax adjustments are read as txt files. Strain-field data from the FOS are available as tsv files.

Catalogs are defined in the class as dictionaries and contain parameter sets (Table 1) for fiber materials, resin materials, winding pins, and winding tools. The parameter sets for frequently used materials and equipment are predefined, while for new ones, the respective class methods (learn-methods, see Table A2) are used to add them. The object catalog includes all currently active objects and their attributes to allow easy data exchange and comparisons. The pyrolysis [49] catalog also comprises a list of previously conducted FVR measurements. Data sets that are imported from a catalog can be overwritten locally in the project file for any object individually.

Table 1. Predefined parameter sets stored in the catalogs of the class definition, see Table A1.

Fiber	Resin	Pins	Tools	Pyrolysis
fiber_product	resin_product	pin_name	tool	pyrolysis_date
fiber_type	mixing_ratio	pin_type	tool_capacity	sample_object
k	viscosity	pin_inner_diameter	nozzle_diameter	sample_location
tex	potlife	pin_outer_diameter		fiber_product
TPM	resin_density	pin_sleeve_diameter		resin_product
fiber_density	resin_correction_factor	pin_height		tool
fiber_tensile_modulus	curing_temp	pin_mass		before_empty
fiber_tensile_strength	curing_min	pin_material		before_with_sample
fiber_max_elongation	resin_price	pin_bolt		after_with_sample
filament_diameter		pin_price		
fiber_price				

Each winding object is stored as a collection of attributes in a centralized curated data storage, where only the basic parameters are saved. Non-fundamental parameters are calculated automatically. During the initialization of an object, all attributes are created and set to None. Subsequently, the methods are used to define the correct parameter values of the attributes step by step. Some parameters are needed in multiple variants,

based on the project phase (justified assumption or direct measurement) or based on the source of data (theoretical calculation or real measurement). All variants of a parameter are stored together in its attribute. The object attributes (Figure 4, Table A1) are structured in groups, including geometrical parameters (graph), fiber material, resin material, winding syntax, hooking syntax, winding pin (anchor), production parameters, physical parameters, mechanical testing, and fiber-optical sensor data.

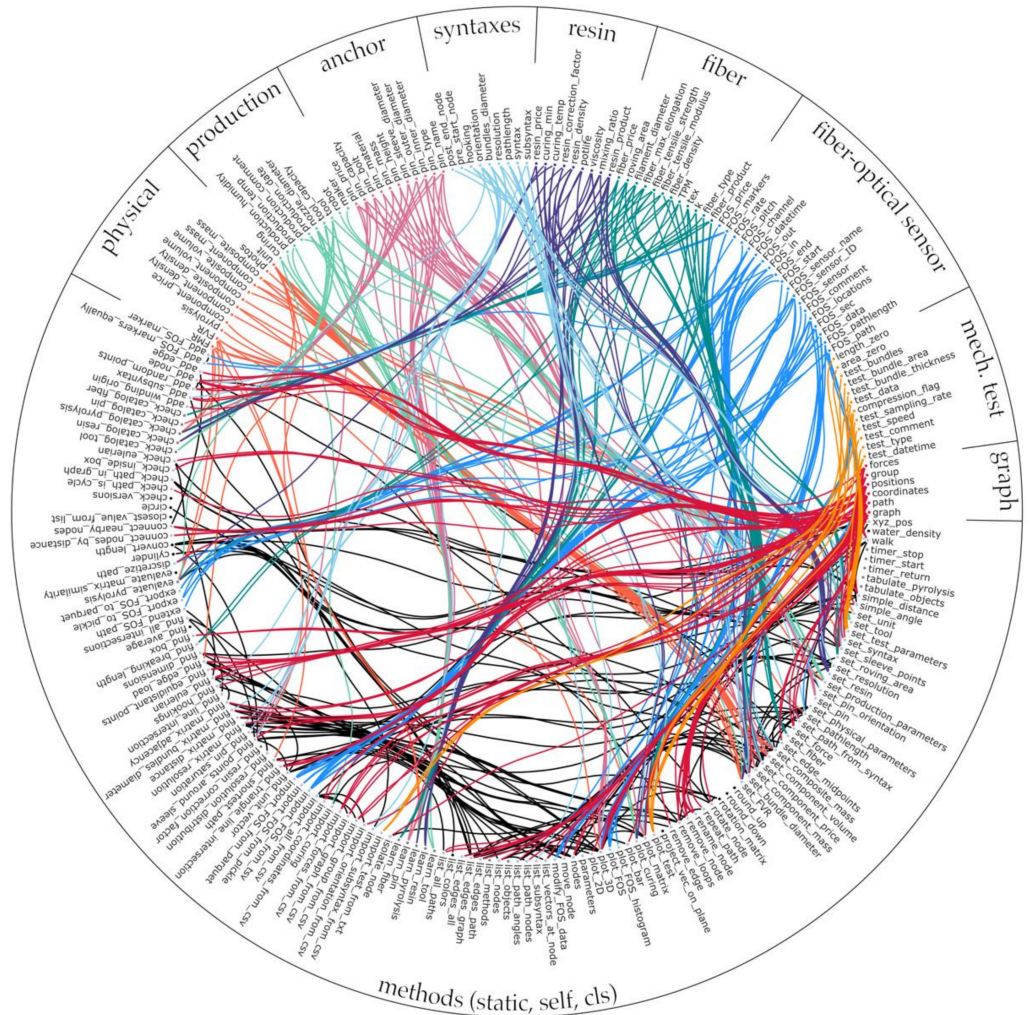


Figure 4. Data flow within the object-oriented design and management tool. The connections are color-coded according to the associated group of attributes. Connections between methods are black. Attributes stored in the catalogs are included.

A variety of specialized methods (Figure 4, Table A2) are included within the CFW class definition that are static or act on the object (self) or on the class (cls). Besides basic functionalities for manipulating the object data, there are also methods that operate in a higher level of detail. Examples include creating a discretized fiber path, performing a framework analysis, obtaining physical parameters, tabulating selected attributes, or plotting them in 2D or 3D. Most of the methods are structured by a leading keyword. Add-methods create an entity within the object model and initialize its parameters. Check-methods evaluate the object parameter without changing them. Find-methods compute object parameters based on other object attributes. Learn-methods add parameters to the catalogs of the class. List-methods collect object parameters in an array-like arrangement. Plot-methods create a visual output for the user. Set-methods overwrite or define the parameters of a single object attribute.

As the graph-theoretical parameters (Figure 4, red group) are the basis of the object model, almost every method accesses these attributes. The other groups of attributes represent certain levels of detail, so the corresponding methods primarily access the respective attributes. An example of this would be the methods and parameters which belong to the fiber-optical sensors group (Figure 4, blue group). In contrast, the analysis- and visualization-methods access a variety of attributes from different groups. Especially the find-methods, which provide higher-level functions, including calls to other methods. Static- and class-methods do not access the attributes of the object. In Figure 4, the set- and learn-methods that read and store parameters in the catalogs (Table 1) are shown with their connection to the corresponding object attributes.

2.2. CFW Design Procedure

The design of a CFW structure mainly focuses on the fiber net form-finding, including the winding and hooking syntax, since it determines the structural performance together with the material parameter. The hooking syntax is a list that enumerates the hooking conditions for each winding step for each anchor [44].

Because it is not economical to compute and evaluate all permutations of the fiber net and the winding plan, the strategy followed in this study was to reduce the design space as best as possible based on an initial design approach. For this, several geometrical-, structural- and fabrication-orientated conditions can be utilized, which must be defined in accordance with the application scenario of the component and fabrication setup. The predefined methods allow the analysis of the winding object to evaluate permutations based on such criteria. Checking the wrapping angles at each node allows evaluating if there are too strong fiber diversions reducing strength (acute angle), or if there is not enough curvature causing fibers to lose contact with the anchors (flat angle). A windability test checks if all the segments along the winding path can be deposited from one or more source points without being blocked by previously placed fiber segments. This is important because CFW does not currently allow fibers to be threaded through. In addition, it is possible to check whether a graph is Eulerian, i.e., whether it has a path that starts and ends at the same node and passes all edges once [50]. This is often desirable in CFW, although multiples greater than one are also relevant. For example, it may happen that a structure must be wound not once but twice to fulfill this criterion (Figure 2). The design process follows a linear procedure with multiple iterations if necessary:

1. Definition of boundary conditions, such as build volume, mass budget, load inductions points, anchor geometry, load cases, center of gravity, and second moments of inertia;
2. Topology optimization (based on voxels or frameworks) to identify the load path for all relevant load cases;
3. Translation of this initial design into a simplified graph (nodes, control points, and edges);
4. Framework analysis to estimate the material distribution for each edge;
5. Creation of the winding syntax and separation in sub syntaxes and bridges;
6. Definition of the anchor orientation and creation of the hooking syntax;
7. Final check if the structure meets the requirements and can be fabricated.

The needed parameters in the first step can be derived from the application of the component. Steps two and three can be done externally based on voxels and then imported via an adapter (`self.import_all_from_csv`, see Table A2), or it can be performed internally using a framework representation of the component. For this, the build volume (`self.find_box`) is randomly filled with points that have a minimum distance to each other (`self.add_random_points`). A graph (Figure 5f) is then created based on adjustable criteria, such as the maximum number of connections or maximum edge length (`self.connect_nearby_nodes`, `self.connect_nodes_by_distance`). Subsequently, paths are determined between the load induction and bearing points for each load case (`self.walk`). Locations with points that are traversed more often than others represent a part of the force flow and are preserved. After all possible pairs of points have been investigated with

sufficient iterations, the paths are superimposed and analyzed by a framework analysis (self.find_edge_load). In step three, less loaded connections are then gradually removed (self.remove_edge), while the remaining control points and node positions are varied slightly (self.move_node) until the iteration reaches an optimum. After the nodes, control points, and graph are set (Figure 5a), the framework analysis (Figure 5b) in step four can also be used to refine the position of control points and nodes or to remove unused sections of the fiber net.

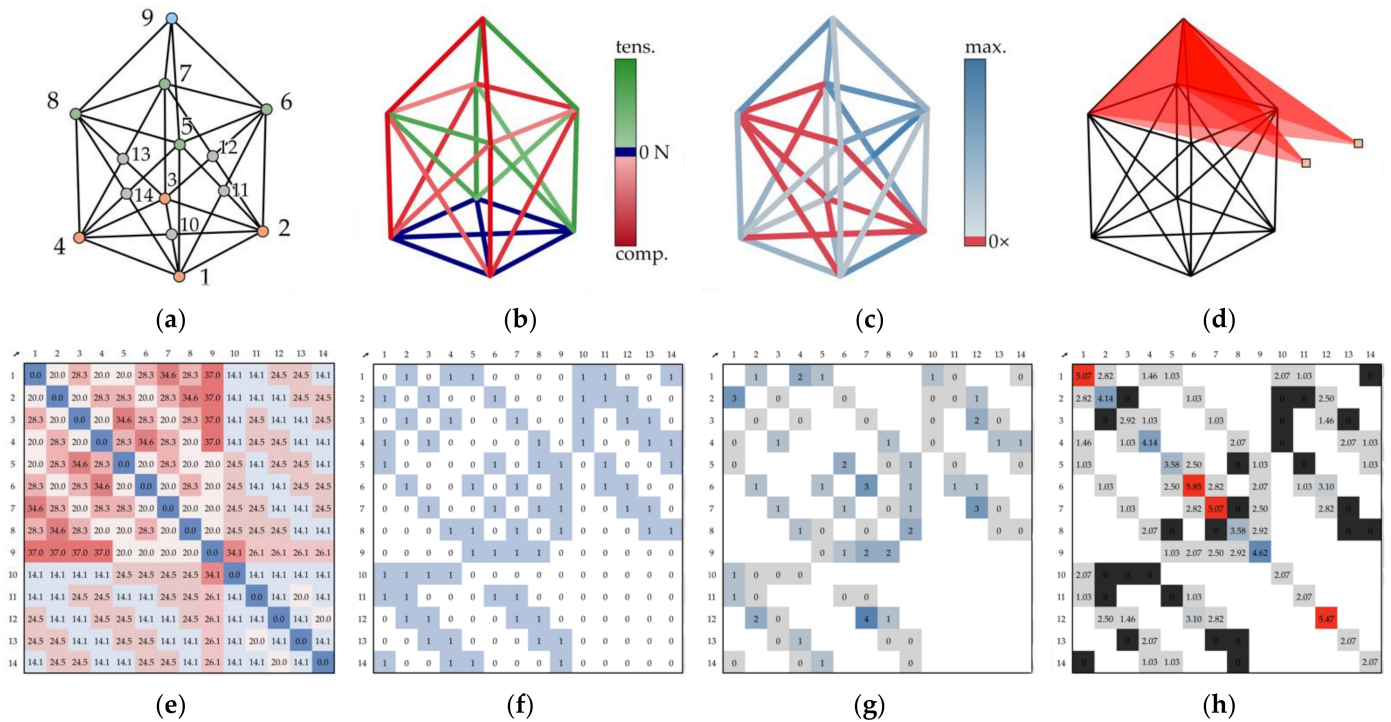


Figure 5. Example visualizations and tables of a generic concise component. (a) Grouped nodes (color-coded), control points (grey) and graph; (b) Framework analysis for a horizontal load in node 9, nodes 1–4 are fixed; (c) Fiber distribution per segment; (d) Windability check, sections 7–9 and 8–9 are not possible to wind from any of the two source points for the given winding syntax; (e) Distance matrix, showing the Euclidean distance between nodes on a blue to red scale; (f) Adjacency matrix, showing the connections of the graph; (g) Resolution matrix, showing the number of fibers per edge taking into account their direction; (h) Bundles diameter matrix, showing the diameter of a theoretical disk that equals the cross-section of all bundles per edge without consideration of their direction, the diagonal shows the winding pin occupancy in the same unit, red anchors are overloaded.

In step five, the winding syntax is designed. This involves the creation of a path, its evaluation, possible adjustments, and the selection of iterations. There are predefined methods (self.find_eulerian, self.list_all_paths) that create possible paths within a given graph. The user then selects a path based on the beforementioned criteria. Alternatively, the user can create paths by repeatedly using the path creation method (self.walk). This method automatically creates a path for a given number of winding steps based on user-defined decision criteria. After each step, the method evaluates which of the remaining edges best matches the current decision criterion and selects it. Thus, the path is created piecewise; however, this does not correspond to the sub syntaxes. The task of the user is to define the decision criterion for each repetition of the path creation method. Possible parameters for the decision criteria are: “towards”, “straight”, “popularity”, and “random”. The “towards” criterion evaluates the current position in the fiber net in relation to a destination node and selects the edge that best points in this direction. The “straight” criterion calculates the direction of the last traveled segment and selects the edge with the least angular deviation from it. The “popularity” criterion selects the edge that leads to the node with the most

or least occupied connections. The “random” criterion selects an eligible edge randomly, which can also be used if another criterion ranks multiple edges as the best option. The path creation method also allows the user to control how often the edges or nodes are allowed to be passed. Another method (`self.find_shortest_path`) can be used to find the shortest path between two nodes, based on the Euclidean distance (`self.simple_distance`) along the traveled edges.

The final winding syntax must meet several criteria. First, the right fiber distribution (Figure 5c) as specified by the framework analysis in step four. Fiber materials with less linear density allow a finer resolution but increase the winding duration proportionally. Another criterion in the winding syntax creation is the occupation (`self.find_pin_saturation`) of the capacity of each anchor element (Figure 5h). If the capacity is exceeded on a single anchor, the fabrication is not feasible. The third criterion is windability (Figure 5d). Here, repositioning the source points can avoid adjustments to the winding syntax. Softer criteria can also help to evaluate the winding syntax, such as the ranges of wrapping angles (`self.list_path_angles`) at each node, fiber traveling direction (Figure 5g), or the maximum permissible length of segments/sections. The fiber traveling direction is relevant for some production setups due to the number of directional reversals. A limitation of the maximum free-spanning fiber length (Figure 5e) is relevant to reduce sagging and for fiber systems that are not able to endure high tensions during winding. After the winding syntax is defined, it can be split into several sub syntaxes and bridges. Bridges are one-time winding sequences that may be executed outside the graph to connect sub syntaxes. They can remain in the component or be removed after fabrication. This division is needed in the case of multi-material components or for multi-stage winding. A winding stage pauses the process to cure the resin and can consist of several sessions.

In step six, the anchors’ orientation is set to match the local fiber net configuration. The hooking condition (`self.find_points_around_sleeve`) of each anchor is defined based on its function (shaping, load induction) and load regime (tension, compression, small or large load). In the last step, final checks are conducted, for example, if the component can be removed from the frame. Then the winding plan (winding and hooking syntax), matrixes (`self.plot_matrix`), and 3D visualizations (`self.plot_3D`), with the information in their correct spatial context, can be exported for production.

2.3. Additively Manufactured Winding Pins

The state-of-the-art winding pin in CFW is a sleeve–washer combination, which restricts the vertical directions from which fiber strands can connect to the anchor element. A new adaptive winding pin was developed [44] that adds individually alignable arms to absorb fibers. They were utilized for this study to allow a direct connection from the upper tension cord to the lower base plate without introducing performance-reducing fiber kinks. A disk at the end of each arm prevents the fiber from slipping off. Recessed measuring tips are located at the outer disk surface as they remain accessible even if the pin is completely filled. Using these tips, the position of the pin can be measured, for example, by means of a robotic system. An additive manufacturing process allows the individualization of each winding pin to optimally suit the local fiber net configuration. The number of arms per pin can be adjusted, and their vertical and horizontal orientations do not have to be a regular pattern. In order to be able to transfer the necessary loads from the bolt connection to the fiber net, the winding pins were made of aluminum alloy powder (AlSi10Mg), utilizing an LPBF machine [51] equipped with a 400 W ytterbium–fiber-laser [52] and application-adjusted settings (Table 2).

Table 2. Machine settings used for the LPBF fabrication of the winding pins.

Parameter	Value	Unit
laser power (max. 400 W)	350	W
laser beam diameter at focal point	80	μm
scan speed	1650	mm/s
hatch distance	130	μm
scan vector length	10	mm
layer thickness	30	μm
build platform preheating temperature	150	$^{\circ}\text{C}$
rotation angle increment	67	$^{\circ}$
fill pattern type	stripes	
inert gas	argon	

The dimensional accuracy of the manufactured winding pins is critical to their function as connectors and fiber anchors. It was evaluated by comparing computer tomography (CT) scans to the CAD model (Figures 6 and 7). The tube of the scanner [53] was set to 225 kV at 597 μA . The volume measurement is calculated by filtered back projection, based on the attenuation of the X-rays due to the object geometry and its material density.

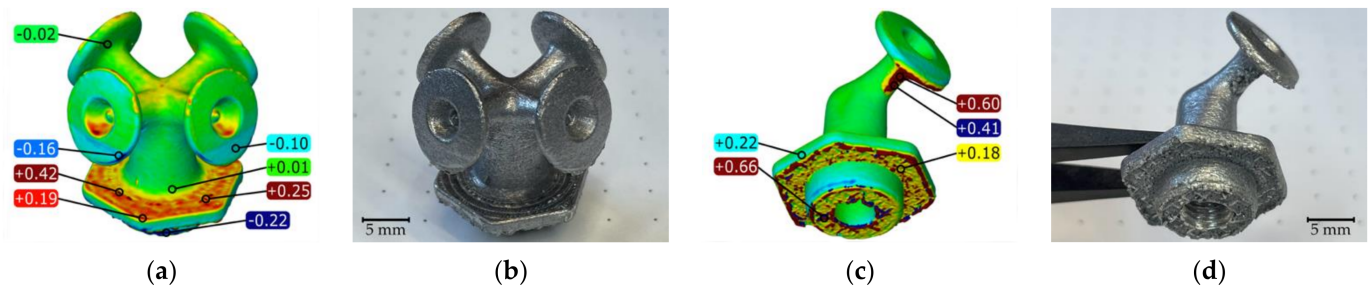


Figure 6. Computer tomography scans of the winding pins. Red areas represent oversized geometry, while blue represent undersized geometry in comparison to the target geometry. (a) CT-scan of the 4-arm winding pin, scale range from -0.2 mm to $+0.2$ mm; (b) Photo of the 4-arm winding pin; (c) CT-scan of the single-arm winding pin, scale range from -0.3 mm to $+0.2$ mm; (d) Photo of the single-arm winding pin.

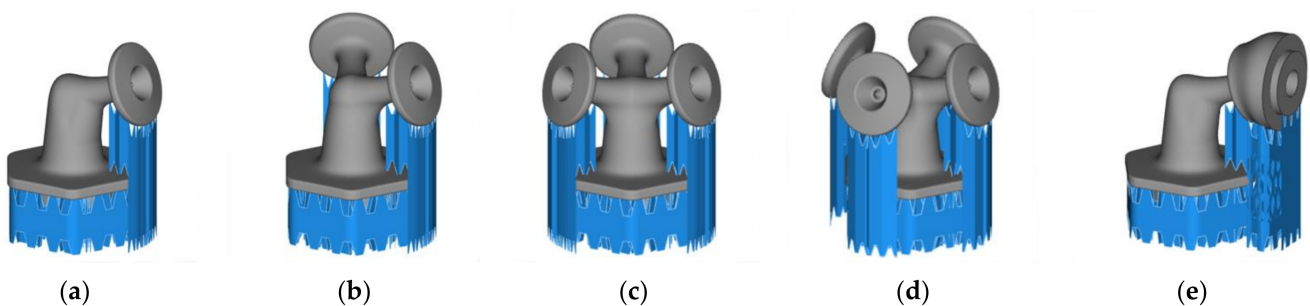


Figure 7. Support structure (blue) needed for the LPBF fabrication process. (a) Single-arm winding pin; (b) 2-arm winding pin; (c) 3-arm winding pin; (d) 4-arm winding pin; (e) Single-arm winding pin with secondary mounting point.

The maximum geometrical deviation of the winding pins caused by surface irregularities was measured to be below 200 μm for the majority of the functional surfaces (Figure 6a). Deviations in this range may be induced by residual thermal stresses occurring during the LPBF fabrication process. Larger deviations (Figure 6c) from the target geometry were generated by remnants of the support structure (Figure 7), which is needed to realize overhangs but also to dissipate process heat. Thus, the positioning of the support structure

in accordance with the process parameters is decisive for the realization of monolithic components with such small dimensions—the outer disk diameter equals 10 mm.

Due to the direct contact of the rovings with the winding pin surfaces, the surface roughness is important to achieve high fiber deposition quality. The surface roughness at the pole of an untreated winding pin is in the range of 30–60 μm (mean arithmetic height). Surface irregularities can damage the roving by cutting filaments during the CFW process in moments of relative movements, especially in a lateral direction. A special winding technique [54] can avoid this by reducing such movements, but it can be laborious to integrate into a robotic CFW process. Therefore, sandblasting and barrel tumbling were investigated (Figure 8). Sandblasting with micro glass beads of 100–200 μm reduced the surface irregularities by 41% and barrel tumbling by 50%, using wet processing deburring powder together with 10 mm plastic cones and tetrahedrons for 8.5 h.

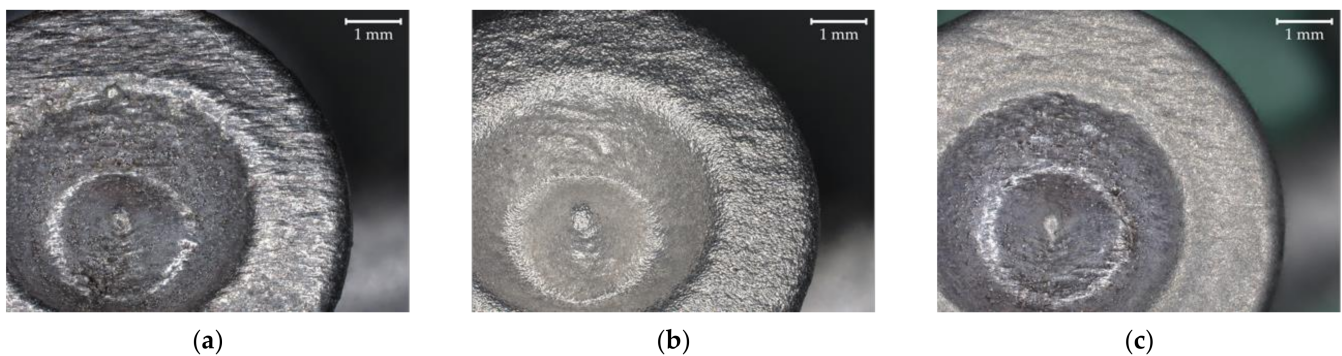


Figure 8. Light microscopic images of the disk area of a 4-arm winding pin. (a) Untreated surface; (b) Sandblasted surface; (c) Surface after barrel tumbling, area around the measuring tip is almost unaffected.

3. Results

3.1. Case Study

In order to present the developed design and management tool and the novel winding pin concept, a case study (Figure 9) was conducted in an engineering application. The objective was to replace an 18.7 kg steel plate with a lighter configuration without reducing dimensional accuracy.

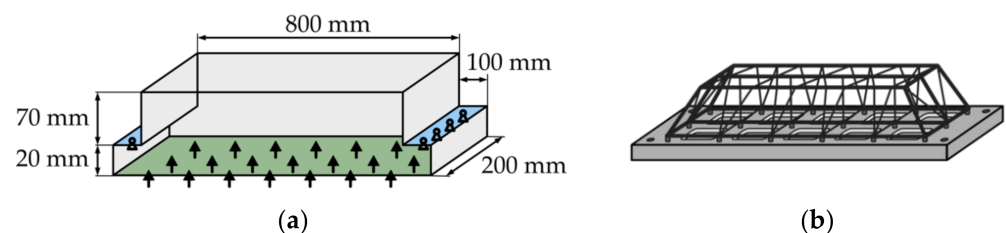


Figure 9. Case study. (a) Build volume, mounting surfaces are marked in blue and load induction surfaces in green; (b) Demonstration component following a hybrid concept, CFRP CFW structure on top of an aluminum base plate connected by LPBF winding pins.

After the design space was defined, a hybrid concept was selected. An aluminum base plate with milled reinforcing ribs connects both mounting surfaces to ensure that the required tolerances are met. A voluminous and lattice carbon-fiber/epoxy-resin CFW structure stiffens the aluminum plate and occupies the previously unused space above the aluminum plate. The LPBF winding pins of the CFW structure join it to the base plate by M5 bolts. The hybrid design allows subsequent machining operations for the tolerance compensation and eliminates the high tolerance requirements for the CFRP component.

3.2. Result of the CFW Design Process

The design of the fiber-reinforced composite component resulted in a configuration similar to a Warren truss [55] but with diagonal internal struts to increase the lateral stiffness (Figure 10a). The digital design tool was used to prepare the winding plan. After identifying winding points, the graph was analyzed (Figure 11b,c), and a winding syntax (Table A3) was created and divided into sub syntaxes for production (Figure 10b–d). Based on the distance matrix (Figure 11a), the lower and upper regions of the component can be identified, and the graph can be derived based on a maximum value of the free-spanning length of a segment. The framework analysis (Figure 10e), together with the resolution matrix and edge bundling plot of the graph, help during the creation of the winding syntax since the user can check the fiber distribution and the connectivity of the component.

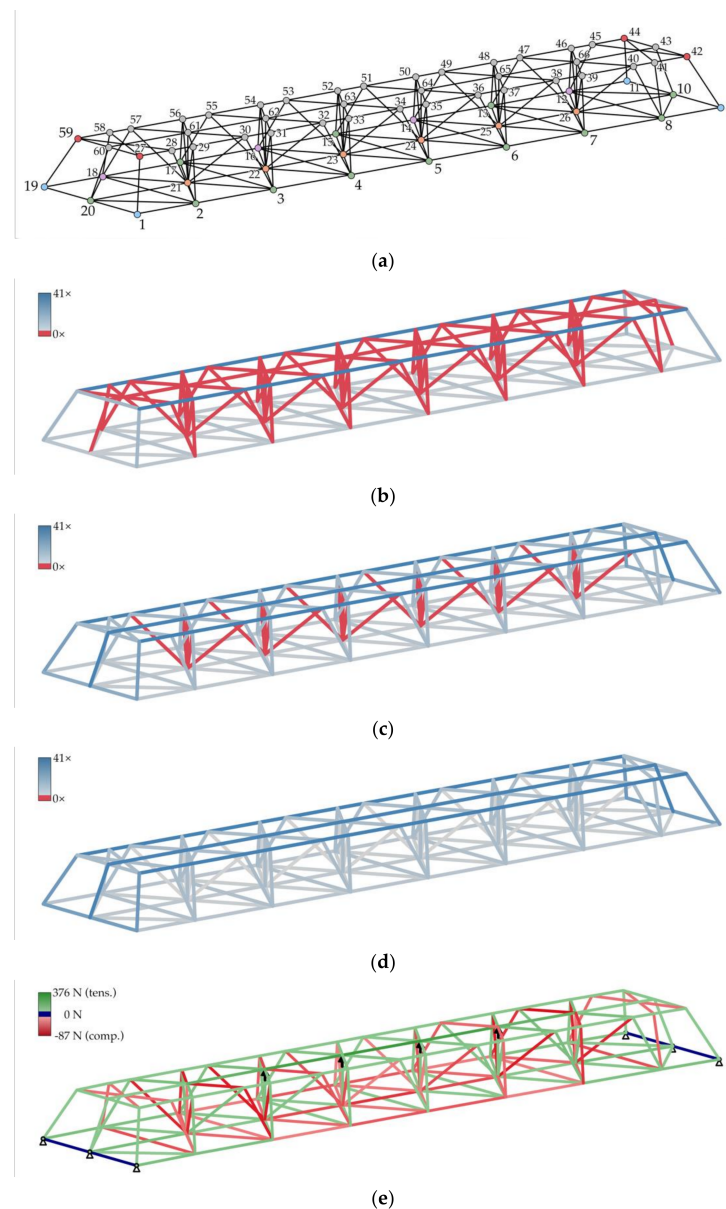


Figure 10. 3D visualization of the fiber-composite structure of the case study. (a) Grouped nodes (color-coded by winding pin type: single-arm (green), 2-arm (blue), 3-arm (red), 4-arm (orange), single-arm pin with secondary mounting point (purple)), control points without winding pins (grey), and graph; (b) Fiber distribution after the first stage; (c) Fiber distribution after the second stage; (d) Fiber distribution after the third stage; (e) Exemplary framework analysis: nodes 62–65 are loaded, whereas nodes 1, 9–11, 19, and 20 are fixed.

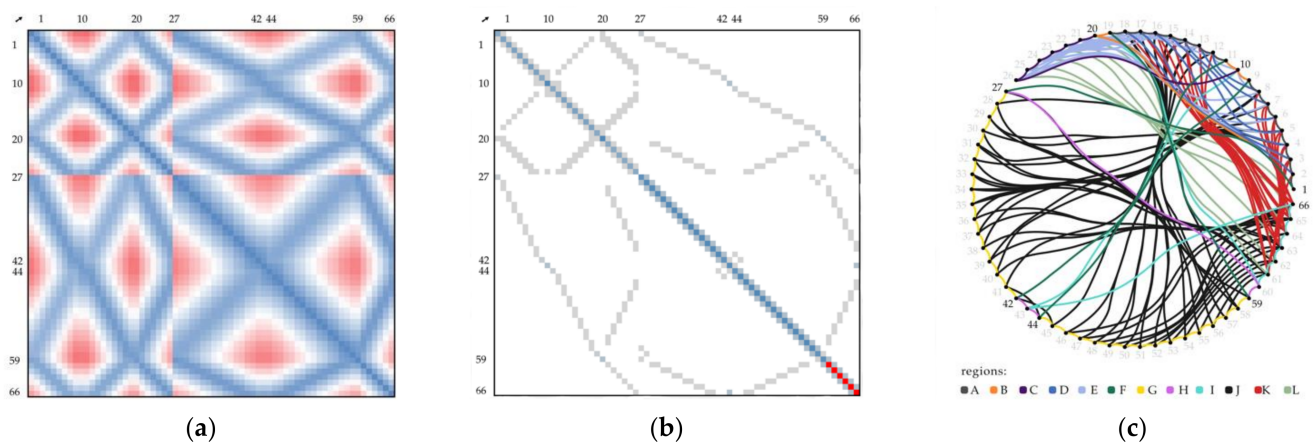


Figure 11. 2D visualization of the fiber-composite structure of the case study with relevant nodes (1, 10, 20, 27, 42, 44, 59, and 66) marked. (a) Distance matrix; (b) Resolution matrix; (c) Edge bundling diagram of the graph color-coded by regions of the fiber net: (A) longer lower outer edge; (B) shorter lower outer edge; (C) lower center rib (section 10–20); (D) lower transverse struts (e.g., section 2–18); (E) lower diagonal ribs; (F) raised outer edges of corners; (G) longer upper outer edge; (H) shorter upper outer edge; (I) upper center rib (section 10–20); (J) lateral cross-bracing; (K) diagonal inner struts; (L) vertical inner struts.

The upper region is located as far away as possible from the base plate and features more material usage than the others component regions to absorb bending loads. Due to the relatively brittle and stiff character of the CFRPs, many winding pins were used to distribute the load as evenly as possible. To prevent the winding fixture from blocking access, the upper region is anchored to only four winding pins, which are only attached during production. This results in a relatively large free-spanning fiber length and a strong fiber–fiber interaction in the upper region. If the entire component were fabricated in one session, the struts placed later would pull the upper region downwards. This deviation from the target geometry is defined by the relation between the fiber tension and free-spanning length. Such a deformation reduces the load-bearing capacity through a loss of structural depth, causes curvature in the tension members, and results in a gradual loss of fiber tension in the previously deposited vertical struts, which may lose contact with each other. For these reasons, the component must be manufactured in a multi-stage process. After the winding of each stage, the resin is cured.

3.3. Multi-Stage CFW Process

For the production, Teijin Tenax-J UMS45 F22 12K [56] carbon fiber with 385 tex at 1.83 g/cm^3 and MGS LR635, MGS LH635, and MGS LH637 [57] epoxy resin by Hexion was used in a 100:10:20 ratio. The fiber was selected because of its comparatively high tensile modulus of 425 GPa. To achieve the highest possible dimensional accuracy of the CFRP component, neither curing the component on the metallic winding fixture nor tempering of the demolded component in an oven was permissible. The aluminum frame could warp due to the high coefficient of thermal expansion, or the CFRP component could distort because of its inhomogeneous material distribution. Consequently, the resin was selected to achieve the highest possible stiffness without temperature treatment. As this resin requires several hours to cure, the time between winding sessions was correspondingly long. An application that allows a fast-curing resin could achieve better cycle times.

The utilized winding equipment was state-of-the-art, except for a modular winding fixture (Figure 12a), which was used to mount the winding pins. It helps to shorten preparation times, maintains relatively high geometrical accuracy, and can be reconfigured easily but restricts the position of the winding pin to a predefined pattern. In the first stage, the lower region was completed, and the two outer tension cords in the upper region were fabricated (Figure 12b). After the first curing, the winding fixture was removed, and in

the second stage, the central tension cords in the top and the lateral diagonal struts were wound (Figure 12c). In the third stage, the inner struts were wound (Figure 12d). Finally, the component was mounted onto the aluminum base plate (Figure 12e).

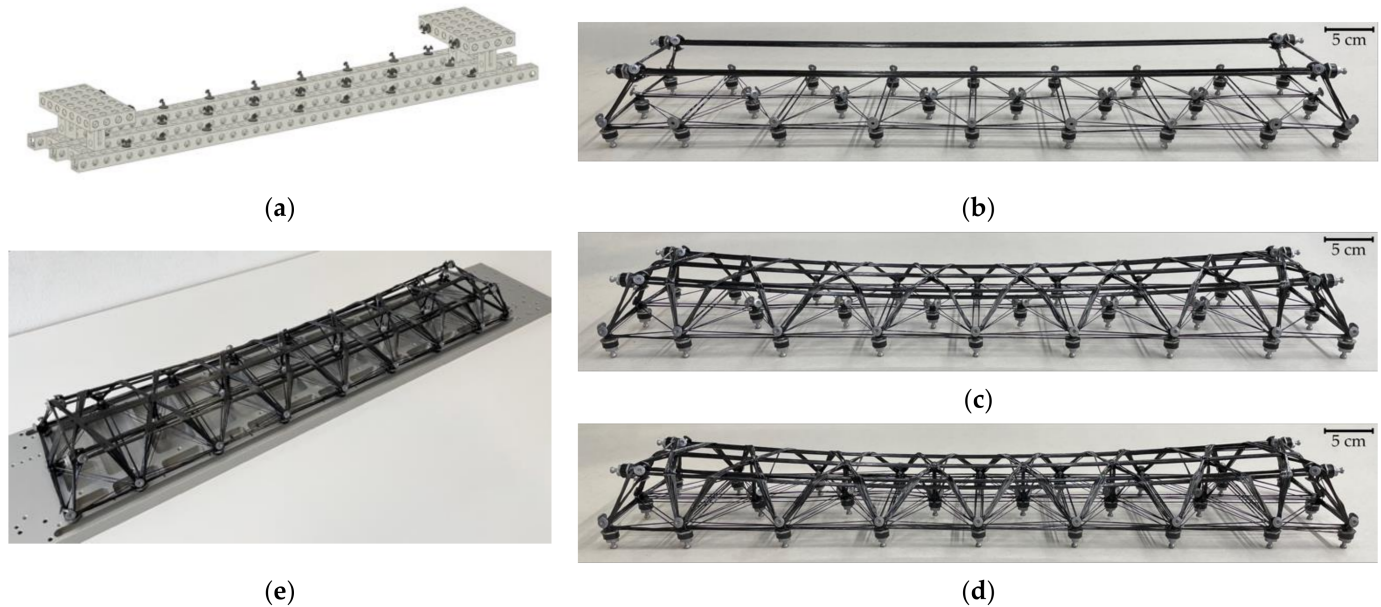


Figure 12. Multi-stage CFW process. (a) CAD of the winding fixture including the winding pins; (b) Photo of the demonstration component after the first winding stage; (c) Photo of the demonstration component after the second winding stage; (d) Photo of the demonstration component after the third winding stage; (e) Photo of the demonstration component after mounting it to the aluminum base plate.

After winding a stage, occasionally, rovings within a segment did not form a coherent bundle. This results mainly from deformations of the fiber net during the stage causing tension loss. To establish a force flow between the rovings, these rovings must be locally bound together with a polytetrafluoroethylene yarn. The yarn can be removed after curing the resin.

The digital design tool allows predicting the material consumption for each production step (Figure 13). From this, the cross-sectional area of each segment of the fiber net can be estimated and used to feed the framework analysis. The FVR is a determining parameter for this calculation and must be estimated a priori. For this, several interrelationships can be used. One of them is deriving it from the fiber and resin parameters and the cross-sectional area at the winding tool nozzle [33]. After each stage, the actual cross-sectional area of each segment was measured by a caliper (Figure 13). The rectangular area obtained by the width and height of the bundles does not represent the cross-sectional area well. A better representation is given by an ellipse or alternatively by a correction factor of $\pi/4$. The difference between the caliper measurements and the prediction results from a local variation in FVR, internal and external voids, and overestimation due to the rugged fiber bundle surface. The standard deviation of the caliper measurements is also predominantly dominated by an irregular division of the fiber bundle into individual bundles.

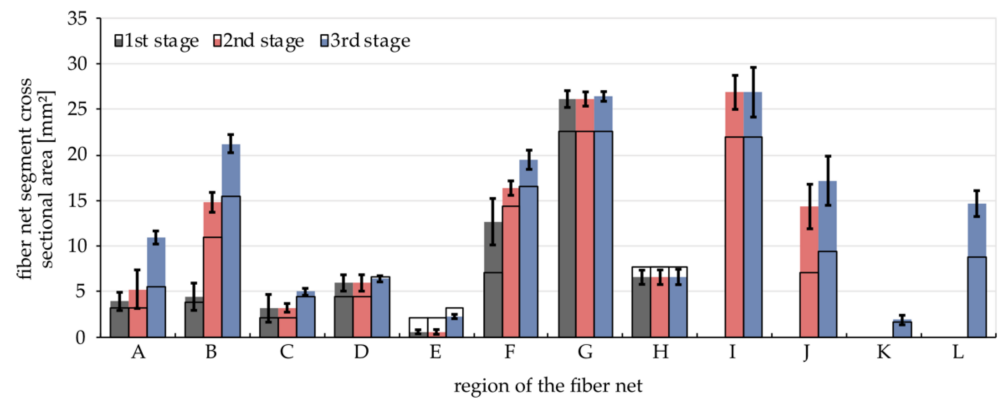


Figure 13. Comparison of the simulated (black outline, FVR of 37.96% based on nozzle diameter) and caliper-measured (colored bars) fiber segment cross-sectional areas for each winding stage. Regions of the fiber net: (A) longer lower outer edge; (B) shorter lower outer edge; (C) lower center rib (section 10–20); (D) lower transverse struts (e.g., section 2–18); (E) lower diagonal ribs; (F) raised outer edges of corners; (G) longer upper outer edge; (H) shorter upper outer edge; (I) upper center rib (section 10–20); (J) lateral cross-bracing; (K) diagonal inner struts; (L) vertical inner struts.

Another method to access the FVR and material consumption of the component is by measuring the resin consumption and total mass of the component (Table 3). This should only be used if negligible amounts of resin are lost during fabrication. From the mass of additional elements, such as winding pins, the composite mass can be calculated, which entails the resin and fiber mass. From this, the FVR can be calculated.

Table 3. Physical parameters of the fiber-composite demonstration component.

	Parameter	Stage 1	Stage 2	Stage 3	Unit
measured	added resin per stage	33.95	29.07	12.77	g
	component mass ¹	250	310	352	g
	composite mass	62	122	164	g
	fiber mass	27.9	58.8	88.1	g
	fiber length	72.4	152.8	228.7	m
	fiber volume ratio	33.28	36.17	41.36	%
predicted	composite mass	74	140	172	g
	fiber mass	28.1	53.1	65.4	g
	fiber length	96.6	182.4	224.7	m
	fiber volume ratio ²	37.96	37.96	37.96	%

¹ including 188.16 g of additional elements, e.g., winding pins. ² same for all phases, since calculated based on the winding tool nozzle diameter.

It can be observed that there is an increase in the measured FVR over the three stages, while the predicted FVR lies in between the extremes of the measured FVR. The increase may be a result of the angular position of the winding tool in relation to the free-spanning fiber during the winding, as higher angles cause lower FVR [33]. The interaction between the winding tool and roving is determined by the winding setup, winding syntax, and trajectory creation method. Based on the linear density of the fiber material, the total fiber length can be calculated and compared to the winding path length of the design tool. This can also be used as a quality control measure to monitor the compliance of the winding plan.

3.4. Mechanical Evaluation

To evaluate the structural performance of the component, two stiffness measurements were conducted. One to measure individual nodes to identify deviations in the fiber net and another measurement to evaluate the stiffness increase of the aluminum base plate by

the fiber-composite structure as well as the performance of the assembled component in relation to the state-of-the-art steel plate reference design. In both cases, several defined forces were applied, and the deformation was measured by one or two dial indicators. This was translated into a spring stiffness.

For the first stiffness evaluation (Figure 14a) on individual winding pins, the fiber-composite structure was mounted to the winding fixture only at nodes 1, 2, 8–12, and 18–20 (Figure 10a). Single winding pins in region A (Figure 11c) were pulled upwards using a spring scale in the force range up to 50 N. On average, spring stiffness of 90.5 ± 23.2 N/mm was measured for an individual pin. Lower values around 75 N/mm were found in the middle, and higher stiffness up to 140 N/mm at the sides. This trend was expected as no pins were fixed in the center, but significant differences in stiffnesses between the front and rear winding pin cluster of region A could be found. This is another quality control measure for monitoring the compliance of the winding plan and for identifying hidden damage or kissing bonds. This approach allows easily localizing weak points, unlike an eigenfrequency measurement by, for example, a laser vibrometer.

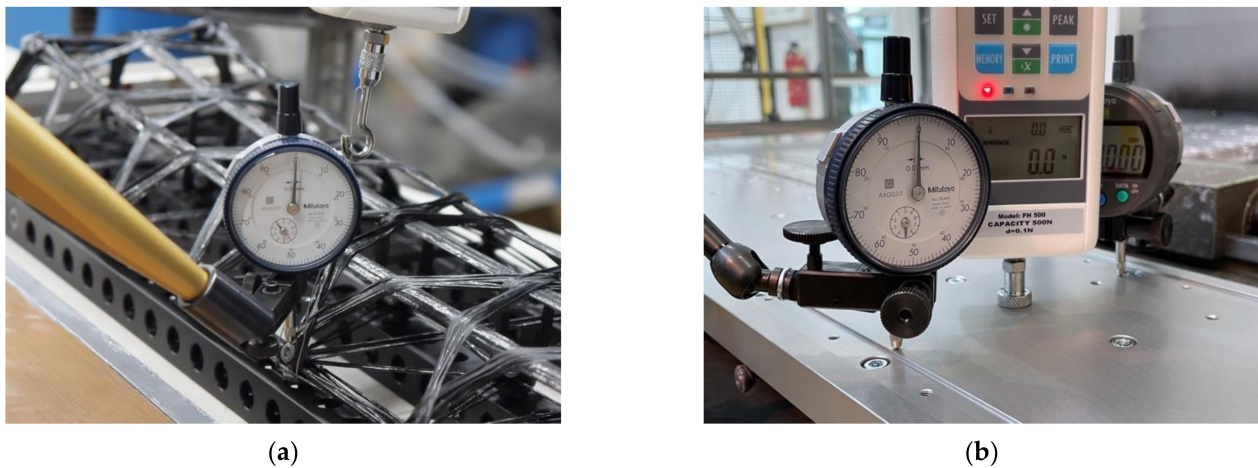


Figure 14. Setups of the force-dependent displacement measurements. (a) Testing of individual winding pins; (b) Testing of the whole assembled component (CFW structure located below the base plate).

For the second stiffness evaluation (Figure 14b) on the component level, the aluminum base plate was supported at its assembly interfaces. The orientation was upside down, neglecting the force of gravity. In a 3-point bending configuration, the plate was loaded in the center (Figure 9a). By installing the fiber-composite structure using all lower winding pins, the stiffness of the aluminum base plate could be increased by a factor of 1.76 in the covered force range up to 100 N. The mass-specific bending stiffness was increased by a factor of 2.5, although the stiffness of the state-of-the-art steel plate reference design remained 81% higher in absolute terms. The absolute mass of the total component in this design was 22% of the original steel component. Of the 4.13 kg component mass, only 0.35 kg is allocated to the fiber-composite structure, including the winding pins with 0.19 kg.

4. Discussion

This study focused on several key aspects to further develop the coreless filament winding process. First, the deployment of a fiber-composite/metal-hybrid concept in an engineering application; second, the implementation of multi-stage winding; and third, the development of a process-specific digital design and management tool that supports all project phases.

The hybrid material and process concept made it possible to combine the individual advantages. The conventionally manufactured metallic components allowed the subsequent machining to obtain the needed tolerances, while the LPBF winding pins enabled

tolerance compensation during the assembly, and the CFW structure introduced high mass-specific stiffnesses into the hybrid component. The hybrid approach could significantly increase the mass-specific stiffness, while an application-specific trade-off between overall mass reduction and total component stiffness must be found individually.

The mechanical performance of the hybrid component depends on the interface between the fiber-composite and metal constituents. In addition, the novel winding pin design allows a more three-dimensional shape of the fiber net without introducing performance-reducing fiber kinks. While the geometric deviations prove to be sufficiently small, the surface roughness of the untreated winding pins could be an obstacle for robotic CFW. Sandblasting could help to improve fiber deposition quality but seems to be economically reasonable only for a smaller number of winding pins, while barrel tumbling primarily affects the exposed surfaces of the pins that are not process relevant.

The introduction of multi-stage winding into CFW simplifies the fabrication process. Despite the division of the demonstration winding into several stages, a deformation of the fiber net produced in the first stage was not completely prevented as nodes 27, 42, 44, and 59 were not fixed during the second stage. If the winding fixture remained attached, the deformation could be further decreased, but it would hinder the winding process in later stages. For the same reason, the winding pins in region C were lifted during the winding of stage 3. At what stage the winding fixture needs to be removed must be decided based on the tolerances and fabrication capabilities. The staging allows the designer increased control over the evolving shape of the component during manufacturing. Thus, the target geometry can be achieved more accurately, resulting in a better match with the digital object model and the simulative predictions. For applications where the achievement of the target geometry depends on this gradual deformation of the fiber net during winding, multi-stage winding offers no advantage.

Multi-stage winding includes further process-related advantages. Errors only affect the current sub syntax and not the entire component. This reduces the number of incorrect components and makes it easier to correct errors while still in production. Errors occur less frequently because the manufacturer must maintain concentration over a shorter period, which is not relevant for robotic winding. Multi-stage winding also allows the use of resins with a shorter pot life, which increases the material selection options. Furthermore, the component can be taken off the winding fixture after the first stage has been wound and cured, simplifying subsequent handling, and reducing cycle times if winding fixture availability is critically limited. A further advantageous aspect of multi-stage winding could be that the first stages of a component are designed to be representative of all further stages and that the component is tested after these first stages. This would allow calibrating simulations with the component-specific values and avoid having to revert to experience with other components. The simulative reproduction of the multi-stage winding process would also make repairs and subsequent reinforcements of CFW structures more understandable. Multi-stage winding may also be combined with multi-material winding.

The developed process-orientated design and management tool acts as a data framework to digitally represent CFW structures. All object data are saved in human-readable form. As the tool is custom-coded, there is full control over the object model and the used methods, which can be customized locally to the individual application scenario. It is intended that data sets can be updated during different project phases, and it distinguishes the data according to their origin (estimation, simulation, measurement). The functionalities of the CFW design tool were demonstrated in the case study, but in its current form, it is primarily a data framework that still offers potential for further methods, object attributes, or even level of details to be included.

Possible aspects to be included in the future, many of which are currently the subject of research, could be a more precise estimation of the winding pin capacity, the automated generation of winding trajectories, including the robot code, topology, and syntax design methods operated by artificial intelligence that do not rely that on human interaction, inclusion of adjacent parts such as the winding fixture or winding pins, simulation methods

that include the wrapping zones and crossing points physically correctly, and fiber–fiber interaction simulation methods depending on the fiber tension during winding. Finally, it would be useful to have a user interface that directly embeds the visualizations, which also still have the potential to be scientifically developed further. Because the tool is research-oriented, it cannot be compared to industrial products in terms of feature set and maintenance, but it was designed specifically for CFW applications, so it is in accordance with the CFW design language and allows a faster and more natural way of interaction.

5. Conclusions

Several interrelated research aspects on coreless filament winding were investigated in the context of a case study in a mechanical engineering application, which demonstrated the functionalities of the digital design tool and validated the synergistic combination of CFW with LPBF and conventional manufacturing methods. This hybrid design approach resulted in an increase in mass-specific stiffness of the case study object and a beneficial combination of several material systems. This could only be achieved by novel winding pins made by additive manufacturing, which prevented geometrical limitations in the fiber net design as they could be customized to their position within the component. The increase in design freedom provided by the pins could only be harnessed because of the digital design tool.

The object-oriented tool helps to design, analyze, visualize, and collect the winding objects in a database in a curated form that operates non-destructively on all levels of detail. It allows to protocol the fabrication and therefore needs to track the origin of the object parameters throughout the project. The digital design tool requires an accurate digital representation of the real structure for reliable analysis and predictions. One approach demonstrated in the case study to improve the digital representation was multi-stage winding. Whereas within a winding stage, the deformation of the fiber net by fiber–fiber interaction takes place, it can be prevented or reduced between winding stages. Multi-stage winding also increases winding fixture availability, simplifies the fabrication process, reduces human errors, and limits the effect of errors to a single stage.

Digital planning is key to an efficient design process for interacting processes and material system in lightweight design. As a foundation, the developed methods provide the holistic digital capturing of the winding objects, which is key to gaining control over the CFW process and optimizing its efficiency for serial production in the future. Only a process with such characteristics may enter an industrial application in engineering.

Author Contributions: Conceptualization, P.M. and R.M.; methodology, P.M., R.M., E.D., C.O. and R.K.; software, P.M.; validation, M.M. and G.T.G.; formal analysis, P.M., R.M. and E.D.; investigation, P.M., R.M., E.D., C.O. and R.K.; resources, M.M. and G.T.G.; data curation, P.M., R.M., E.D., C.O. and R.K.; writing—original draft preparation, P.M. and C.O.; writing—review and editing, R.M., E.D., C.O. and R.K.; visualization, P.M., R.M. and R.K.; supervision, M.M. and G.T.G.; project administration, M.M.; funding acquisition, P.M., R.M. and M.M. All authors have read and agreed to the published version of the manuscript.

Funding: This research was funded by the Ministry of Science, Research and the Arts of Baden-Wuerttemberg (MWK, Ministerium für Wissenschaft, Forschung und Kunst Baden-Württemberg).

Data Availability Statement: The data presented in this study are available on request from the corresponding author. The data are not publicly available due to third party restrictions.

Acknowledgments: The authors would like to express their gratitude towards their fellow researchers Peter Hoffrogge, Thomas Götz, Daniel Müller, and Robert Wegner.

Conflicts of Interest: The authors declare no conflict of interest. The funders had no role in the design of the study; in the collection, analyses, or interpretation of data; in the writing of the manuscript, or in the decision to publish the results.

Appendix A

Table A1. Predefined attributes of a winding object in groups: geometrical parameters, mechanical testing data, fiber-optical sensor data, fiber material, resin material, winding and hooking syntaxes, winding pin attributes, production and physical parameters.

Attribute (self.)	Data Type *	Dimension	Description
ID	str	-	name of the winding object
graph	dict of int: list of int	-	connections between nodes
path	list of int	-	nodes along the fiber path
coordinates	dict of int: tuple of float	self.unit	x, y, and z coordinates of nodes
positions	dict of str: tuple of float	self.unit	x, y, and z coordinates of control points
group	dict of str: str	-	groups of the nodes (color names)
forces	dict of int: tuple of float	kN	x, y, and z components of external forces acting on nodes
test_datetime	datetime.datetime	date, time	local date and time of the start of the mechanical test
test_type	str	-	type of mech. test: tension, compression, or 3P-bending
test_comment	str	-	special test parameters or settings and observations
test_speed	float	mm/min	speed of the cross head (if constant, otherwise: 0)
test_sampling_rate	float	Hz	samples per seconds of the universal testing machine
compression_flag	bool	-	if true, mirrors the force-displacement-graphs
test_data	pandas.dataframe	multiple	data of mech. test: time, force, displacement, stress, and strain
test_bundle_thickness	list of float	mm	measured width and depth of the relevant bundle(s)
test_bundle_area	float	mm ²	area of relevant bundle(s), e.g., obtained by micro-sections
test_bundles	int	-	number of bundles in the tested cross-section
area_zero	float	mm ²	initial cross-section area of the component
length_zero	float	mm	initial length of the test specimen in testing direction
FOS_path	list of int	-	nodes along the FOS path
FOS_pathlength	dict of str: float	m	length of FOS path (theor. / real and simple/discretized)
FOS_data	pandas.dataframe	multiple	FOS data set (strain over time and fiber length)
FOS_sec	list of float	sec	timesteps of the FOS measurements
FOS_locations	list of float	m	locations of the sampling points along the FOS
FOS_comment	str	-	special test parameters or settings and observations
FOS_sensor	str	-	type of used FOS
FOS_sensor_ID	str	-	ID of the FOS as given by the FOS system
FOS_sensor_name	str	-	description of the FOS as given by the FOS system
FOS_start	float	m	position along the FOS where the measurement zone starts
FOS_end	float	m	position along the FOS where the measurement zone ends
FOS_in	float	m	position along the FOS where it enters the component
FOS_out	float	m	position along the FOS where it leaves the component
FOS_datetime	datetime.datetime	date, time	date and time of the start of the FOS measurement (UTC)
FOS_channel	int	-	channel the FOS was attached to
FOS_pitch	float	mm	distance between two adjacent sampling points
FOS_rate	float	Hz	sampling rate of the FOS system
FOS_markers	dict of str: list of float	m	relevant sections along the FOS
FOS_price	float	€/m	price of the FOS
fiber_product	str	-	name of the fiber product
fiber_type	str	-	type of the fiber, e.g., carbon, glass, or flax
k	int	1000	number of the filaments, e.g., 6, 12, 24, or 48
tex	int	g/km	linear density of the fiber roving or yarn
TPM	float	1/m	number of twists per meter
fiber_density	float	g/cm ³	density of the dry fiber material
fiber_tensile_modulus	float	GPa	tensile modulus of the dry fiber
fiber_tensile_strength	float	MPa	tensile strength of the dry fiber
fiber_max_elongation	float	%	elongation at failure
filament_diameter	float	µm	average diameter of a single filament/fiber
roving_area	float	mm ²	cross-sectional area of the dry fiber roving or yarn
fiber_price	float	€/g	price of the fiber product
resin_product	str	-	name of the resin product
mixing_ratio	dict of str: float	%	ingredients of the resin and their mixing ratios
viscosity	int	mPa *s	viscosity of the mixed resin at room temperature
potlife	int	min	pot life of the mixed resin
resin_density	float	g/cm ³	density of the cured resin
resin_correction_factor	float	%	correction factor for the pyrolysis [49]
curing_temp	list of int	°C	temperature level for resin curing and tempering
curing_min	list of int	min	duration of the steps to cure the resin
resin_price	float	€/g	price of the resin product

Table A1. Cont.

Attribute (self.)	Data Type *	Dimension	Description
subsyntax	dict of str: list of int	-	named sequences of nodes
syntax	list of str or int	-	list containing keys of the sub syntax or the node sequence
pathlength	dict of str: float	unit	length of fiber path (theor. / real and simple/discretized)
resolution	dict of tuple of int: int	-	number of bundles at each edge
bundles_diameter	dict of tuple of int: float	mm	theoretical diameter of bundles at each edge and winding pin
orientation	dict of int: tuple of float	-	unit vectors of the axial direction of each winding pin
hooking	list of int	-	number of hookings performed on each winding pin, see [44]
pre_start_node	int or list of float	multiple	additional start node (int/-) or coordinates (list of float/unit)
post_end_node	int or list of float	multiple	additional end node (int/-) or coordinates (list of float/unit)
pin_name	str	-	name of the winding pin
pin_type	str	-	type of the winding pin, e.g., sleeve–washer combination
pin_inner_diameter	float	mm	inner diameter of the winding pin
pin_outer_diameter	float	mm	outer diameter of the winding pin
pin_sleeve_diameter	float	mm	inner diameter of the sleeve
pin_height	float	mm	height of the sleeve
pin_mass	float	g	mass of the winding pin parts that remain in the component
pin_material	str	-	material of the winding pin parts that remain in the component
pin_bolt	str	-	nominal diameter of the center bolts thread
pin_capacity	float	mm	capacity of the winding pin expressed as a diameter
pin_price	float	€	price of the single-use parts of the winding pin
maker	list of str	-	operator name(s)
robot	str	-	robot type or serial number or “manual” keyword
tool	str	-	name of the used winding tool
tool_capacity	float	ml	volume of resin that the tool can hold without reloading
nozzle_diameter	float	mm	diameter of the characteristic tool opening
production_date	datetime.date	date	date of winding
production_comment	str	-	special production parameters or settings and anomalies
production_temp	float	°C	temperature of the production environment
production_humidity	float	%	relative humidity of the production environment
curing	pandas.dataframe	multiple	temperature curve of the curing process
unit	str	multiple	defines the unit of length of the winding object model
photos	list of str	-	file names of pictures or videos related to the winding object
composite_mass	dict of key: float	g	mass of the composite of the component (theor., real)
component_mass	dict of key: float	g	mass of the whole component (keys: theor., real)
composite_volume	float	cm ³	volume of the composite of the component (key set by mass)
component_volume	float	cm ³	volume of the whole component (key set by mass)
composite_density	float	g/cm ³	density of the composite of the component (key set by mass)
component_density	float	g/cm ³	density of the whole component (key set by mass)
component_price	dict of key: float	€	material price of the whole component (keys: theor., real)
pyrolysis	datetime.date	date	date of the pyrolysis measurement
FVR	float	%	characteristic fiber volume ratio of the winding object
FMR	float	%	characteristic fiber mass ratio of the winding object

* Data types are indicated as follows: integer (int), floating-point numbers (float), boolean (bool), string (str), list (list), tuple (tuple), and dictionary with key and value (dict of key: value).

Table A2. Predefined methods of the winding class.

Type *	Name	Description
self	__len__	returns the number of missing attributes of the winding object
self	__str__	returns all variables of the winding object
self	add_FOS_marker	adds a marker to FOS data
self	add_FOS_markers_equally	adds equally spaced markers
self	add_edge	adds one or multiple edges to the graph
self	add_node	adds a node to the winding object
self	add_random_points	adds random points inside a single or multiple boxes
self	add_subsyntax	adds a node sequence to the sub syntaxes
self	add_winding_origin	adds a winding origin for the windability check
cls	check_catalog_fiber	returns the control string for a fiber of the catalog
cls	check_catalog_pin	returns the control string for a winding pin of the catalog
cls	check_catalog_pyrolysis	returns the control string for a pyrolysis measurement of the catalog

Table A2. Cont.

Type *	Name	Description
cls	check_catalog_resin	returns the control string for a resin of the catalog
cls	check_catalog_tool	returns the control string for a fiber of the catalog
self	check_eulerian	checks if the graph is Eulerian (Hierholzer's algorithm)
self	check_inside_box	checks if a point is inside a box
self	check_path_in_graph	checks if the path is a subset of the graph
self	check_path_is_cycle	checks if the first and last node within the path are the same
static	check_versions	checks the versions of the included Python packages
static	circle	returns the coordinates of a circle
static	closest_value_from_list	returns the closest value to the given value that is part of a list
self	connect_nearby_nodes	connects all nodes with their closest nodes at a given number of edges per node
self	connect_nodes_by_distance	connects all nodes within a given Euclidian distance
static	convert_length	converts values of length between μm , mm, cm, dm, m, and km
static	cylinder	returns the coordinates of a cylinder
self	discretize_path	discretizes a winding path at a winding pin
static	evaluate_matrix_similarity	returns the number of changes necessary to make both matrixes the same
cls	evaluate_pyrolysis	evaluates pyrolysis data and returns fiber volume ratio and fiber mass ratio
self	export_FOS_to_parquet	exports FOS data as a parquet file (slow but small file)
self	export_FOS_to_pickle	exports FOS data as pickle file (fast but large file)
self	extend_FOS_path	extends the FOS path around sleeve points
self	find_all_intersections	finds all intersections in a graph
static	find_average	returns the weighted average of values
self	find_box	finds the corner points of a box from a given center point
self	find_breaking_length	returns the breaking length in km of the dry fiber material
self	find_dimensions	returns the overall dimensions of the winding object
self	find_edge_load	performs a framework analysis of the winding object
self	find_equidistant_points	returns a list of equidistant points between two nodes
self	find_eulerian	returns a Eulerian path or cycle of the graph
self	find_hookings	returns a dictionary with the hooking condition parameter [44] per node in winding order
self	find_line_intersection	finds the intersection point of two lines between nodes
self	find_matrix_adjacency	returns the adjacency matrix for the graph
self	find_matrix_bundles_diameter	returns the bundles diameter matrix
self	find_matrix_distance	returns the distance matrix ignoring the graph
self	find_matrix_resolution	returns the resolution matrix
self	find_pin_saturation	returns the theoretical occupancy of each winding pin in percent
self	find_points_around_sleeve	returns points around a winding sleeve
cls	find_resin_correction_factor	returns the resin correction factor used in the pyrolysis [49]
self	find_resolution_distribution	returns the undirected winding resolution distribution
self	find_shortest_path	returns the shortest path between two given nodes
self	find_triangle_line_intersection	returns the position of a line intersecting a triangle given by three points
self	find_unit_vector	returns the unit vector between two nodes or positions
self	import_FOS_from_parquet	imports FOS data from a gzip file
self	import_FOS_from_pickle	imports FOS data from a gzip file
self	import_FOS_from_tsv	imports FOS data from a tsv file created by the FOS system
self	import_all_from_csv	imports the graph, groups, and coordinates from csv file
self	import_coordinates_from_csv	imports the node coordinates from a csv file
self	import_curing	imports the curing temperature curve from a csv file
self	import_forces_from_csv	imports the forces acting on the nodes from a csv file
self	import_graph_from_csv	imports the graph from a csv file
self	import_group_from_csv	imports the color groups of the nodes from a csv file
self	import_orientation_from_csv	imports the winding pin orientations from a csv file
self	import_subsyntax_from_csv	imports the sub syntaxes from a csv file
self	import_test_from_txt	imports mechanical testing data from a txt file created by the universal testing machine
self	isolate_node	isolates a node
cls	learn_fiber	adds a fiber to the fiber catalog of the class
cls	learn_pin	adds a winding pin to the winding pin catalog of the class
cls	learn_pyrolysis	adds a pyrolysis measurement to the pyrolysis catalog of the class

Table A2. Cont.

Type *	Name	Description
cls	learn_resin	adds a resin to the resin catalog of the class
cls	learn_tool	adds a tool to the tool catalog of the class
self	list_all_paths	lists paths between two nodes that does not contain cycles or loops
static	list_colors	lists the predefined colors
self	list_edges_all	lists all possible edges ignoring the graph
self	list_edges_graph	lists all edges within the graph
self	list_edges_path	lists the edges along the path
cls	list_methods	lists all methods
self	list_nodes	lists all nodes in the graph
cls	list_objects	lists all winding objects of the class
self	list_path_angles	lists all angles at nodes along the path
self	list_path_nodes	lists the nodes traveled by the path, including how often they have been visited
self	list_subsyntax	returns a list of all sub syntaxes
self	list_vectors_at_node	lists the unit vectors of a node
self	modify_FOS_data	limits, crops the array in time or space, smooths FOS data, and replaces NaNs by zeros
self	move_node	shifts or relocates a node
self	nodes	returns the number of nodes in the graph or coordinates
self	parameters	returns a list of all parameters of the winding object
self	plot_2D	plots the winding object in 2D
self	plot_3D	plots the winding object in 3D
self	plot_FOS	plots the FOS data as surface plot, matrix plot, or 2D plot
self	plot_FOS_histogram	plots a histogram of the FOS data
self	plot_bar	plots a bar chart of a list
self	plot_curing	plots curing data
self	plot_matrix	plots a matrix
self	plot_test	plots the mech. test data as force-displacement or stress-strain diagram
static	project_vec_on_plane	projects a vector onto a plane
self	remove_edge	removes a specific edge
self	remove_loops	removes all loops in the graph and/or path
self	remove_node	removes a specific node
self	rename_node	renames a node
self	repeat_path	repeats the path
self	rotate_node	rotates a node or list of nodes around a point and vector in counterclockwise direction
static	rotation_matrix	returns the rotation matrix of a counterclockwise rotation about the axis
static	round_down	rounds down a number at a decimal
static	round_up	rounds up a number at a decimal
self	set_FVR	sets the FVR value of the winding object from the pyrolysis catalog or overrides it manually
self	set_bundle_diameter	sets the bundles diameter and the winding pin occupation
self	set_component_mass	sets the component mass of the winding object
self	set_component_price	sets the price of the component including sleeves and FOS
self	set_component_volume	sets the volume of the component measured by Archimedes' principle
self	set_composite_mass	sets the composite mass of the component
self	set_edge_midpoints	sets the positions of the midpoints of all edges of the graph and adds them to self.positions
self	set_fiber	sets the fiber material of the winding object based on the fiber catalog of the class
self	set_force	set the force of a node
self	set_path_from_syntax	sets the path based on self.syntax
self	set_pathlength	calculates the theoretical length of the fiber or FOS path
self	set_physical_parameters	set the composite and component mass as well as the component price
self	set_pin	sets the resin material of the winding object based on the resin catalog of the class
self	set_pin_orientation	sets the winding pin orientation by a path segment
self	set_production_parameters	sets the parameters of the production or overrides them
self	set_resin	sets the resin material of the winding object based on the resin catalog of the class
self	set_resolution	sets the resolution (bundles per segment) of the winding object

Table A2. Cont.

Type *	Name	Description
self	set_oving_area	sets the cross-sectional area in mm ² of a dry roving by filament number or linear density
self	set_sleeve_points	sets the in and out points of a node with given sleeve parameters
self	set_syntax	sets the syntax of the winding object
self	set_test_parameters	sets the parameters of the mechanical test or overrides them
self	set_tool	sets the winding tool based on the tool catalog of the class
self	set_unit	sets the unit of length for the node coordinates
self	simple_angle	returns the included angle at the left node of a list of three nodes
self	simple_distance	returns the Euclidean distance between two nodes
cls	tabulate_objects	returns a table of selected parameters of all winding objects of the class
cls	tabulate_pyrolysis	returns a table of selected parameters of all pyrolysis measurements of the class
cls	timer_return	prints a timer
cls	timer_start	starts a timer
cls	timer_stop	stops a timer
self	walk	sets a path based on the graph and the selected method of traveling
static	water_density	returns the density of water depending on the water temperature
self	xyz_pos	returns the x, y, and z coordinates of a node or position

* Method types are indicated as follows: depended on the object (self), depending on the class (cls), and static methods (static).

Table A3. Winding syntax of the demonstration component.

Stage	Sub Syntax	Regions *	Repetitions	Sequence
1	1	A, B	2×	20, 1, 2, 3, 4, 5, 6, 7, 8, 9, 10, 11, 12, 13, 14, 15, 16, 17, 18, 19, 20
	2	A, B, D	2×	20, 1, 2, 18, 2, 3, 17, 3, 4, 16, 4, 5, 15, 5, 6, 14, 6, 7, 13, 7, 8, 12, 8, 9, 10, 11, 12, 8, 12, 13, 7, 13, 14, 6, 14, 15, 5, 15, 16, 4, 16, 17, 3, 17, 18, 2, 18, 19, 20
	3	A, B, C	2×	20, 21, 22, 23, 24, 25, 26, 10, 11, 12, 13, 14, 15, 16, 17, 18, 19, 20, 1, 2, 3, 4, 5, 6, 7, 8, 9, 10, 26, 25, 24, 23, 22, 21, 20
	4	E	4×	20, 18, 21, 3, 22, 16, 23, 5, 24, 14, 25, 7, 26, 12, 10, 8, 26, 13, 25, 6, 24, 15, 23, 4, 22, 17, 21, 2, 20
	bridge	B	1×	20, 19
	5	F	6×	19, 59, 19
	bridge	B, F, G, H	1×	19, 59, 58, 57, 56, 55, 54, 53, 52, 51, 50, 49, 48, 47, 46, 45, 44, 11, 10, 9, 42, 43, 44
	6	F	6×	44, 11, 44
	7	G	20×	44, 45, 46, 47, 48, 49, 50, 51, 52, 53, 54, 55, 56, 57, 58, 59, 58, 57, 56, 55, 54, 53, 52, 51, 50, 49, 48, 47, 46, 45, 44
	bridge	H	1×	44, 43, 42
	8	F	6×	42, 9, 42
	9	H	6×	42, 43, 44, 43, 42
	10	G	20×	42, 41, 40, 39, 38, 37, 36, 35, 34, 33, 32, 31, 30, 29, 28, 27, 28, 29, 30, 31, 32, 33, 34, 35, 36, 37, 38, 39, 40, 41, 42
bridge	G	1×	42, 41, 40, 39, 38, 37, 36, 35, 34, 33, 32, 31, 30, 29, 28, 27	
11	H	7×	27, 60, 59, 60, 27	
12	F	6×	27, 1, 27	
bridge	B	1×	27, 1, 20	
2	13	B, F, J	10×	20, 1, 27, 58, 18, 57, 61, 30, 3, 31, 62, 54, 16, 53, 63, 34, 5, 35, 64, 50, 14, 49, 65, 38, 7, 39, 66, 46, 12, 45, 42, 9, 10, 11, 44, 41, 8, 40, 66, 47, 13, 48, 65, 37, 6, 36, 64, 51, 15, 52, 63, 33, 4, 32, 62, 55, 17, 56, 61, 29, 2, 28, 59, 19, 20
	14	I	20×	20, 60, 61, 62, 63, 64, 65, 66, 43, 10, 43, 66, 65, 64, 63, 62, 61, 60, 20
	13	B, F, J	3×	20, 1, 27, 58, 18, 57, 61, 30, 3, 31, 62, 54, 16, 53, 63, 34, 5, 35, 64, 50, 14, 49, 65, 38, 7, 39, 66, 46, 12, 45, 42, 9, 10, 11, 44, 41, 8, 40, 66, 47, 13, 48, 65, 37, 6, 36, 64, 51, 15, 52, 63, 33, 4, 32, 62, 55, 17, 56, 61, 29, 2, 28, 59, 19, 20

Table A3. Cont.

Stage	Sub Syntax	Regions *	Repetitions	Sequence
3	15	B, F, J, L	1×	20, 1, 27, 58, 18, 57, 61, 21, 61, 30, 3, 31, 62, 22, 62, 54, 16, 53, 63, 23, 63, 34, 5, 35, 64, 24, 64, 50, 14, 49, 65, 25, 65, 38, 7, 39, 66, 26, 66, 46, 12, 45, 42, 9, 10, 11, 44, 41, 8, 40, 66, 26, 66, 47, 13, 48, 65, 25, 65, 37, 6, 36, 64, 24, 64, 51, 15, 52, 63, 23, 63, 33, 4, 32, 62, 22, 62, 55, 17, 56, 61, 21, 61, 29, 2, 28, 59, 19, 20
	16	B, F, J, K, L	3×	20, 1, 27, 58, 18, 57, 21, 61, 21, 30, 3, 31, 22, 62, 22, 54, 16, 53, 23, 63, 23, 34, 5, 35, 24, 64, 24, 50, 14, 49, 25, 65, 25, 38, 7, 39, 26, 66, 26, 46, 12, 45, 42, 9, 10, 11, 44, 41, 8, 40, 26, 66, 26, 47, 13, 48, 25, 65, 25, 37, 6, 36, 24, 64, 24, 51, 15, 52, 23, 63, 23, 33, 4, 32, 22, 62, 22, 55, 17, 56, 21, 61, 21, 29, 2, 28, 59, 19, 20
	1	A, B	1×	20, 1, 2, 3, 4, 5, 6, 7, 8, 9, 10, 11, 12, 13, 14, 15, 16, 17, 18, 19, 20
	2	A, B, D	1×	20, 1, 2, 18, 2, 3, 17, 3, 4, 16, 4, 5, 15, 5, 6, 14, 6, 7, 13, 7, 8, 12, 8, 9, 10, 11, 12, 8, 12, 13, 7, 13, 14, 6, 14, 15, 5, 15, 16, 4, 16, 17, 3, 17, 18, 2, 18, 19, 20
	4	E	2×	20, 18, 21, 3, 22, 16, 23, 5, 24, 14, 25, 7, 26, 12, 10, 8, 26, 13, 25, 6, 24, 15, 23, 4, 22, 17, 21, 2, 20
	17	C	2×	20, 21, 22, 23, 24, 25, 26, 10, 26, 25, 24, 23, 22, 21, 20
	1	A, B	2×	20, 1, 2, 3, 4, 5, 6, 7, 8, 9, 10, 11, 12, 13, 14, 15, 16, 17, 18, 19, 20

* Regions of the fiber net: (A) longer lower outer edge; (B) shorter lower outer edge; (C) lower center rib (section 10–20); (D) lower transverse struts (e.g., section 2–18); (E) lower diagonal ribs; (F) raised outer edges of corners; (G) longer upper outer edge; (H) shorter upper outer edge; (I) upper center rib (section 10–20); (J) lateral cross-bracing; (K) diagonal inner struts; (L) vertical inner struts.

References

- Bakis, C.E.; Bank, L.C.; Brown, V.L.; Cosenza, E.; Davalos, J.F.; Lesko, J.J.; Machida, A.; Rizkalla, S.H.; Triantafillou, T.C. Fiber-Reinforced Polymer Composites for Construction—State-of-the-Art Review. *J. Compos. Constr.* **2002**, *6*. [\[CrossRef\]](#)
- Utsunomiya, S.; Kamiya, T.; Shimizu, R. Development of CFRP mirrors for space telescopes. In Proceedings of the Volume 8837—Material Technologies and Applications to Optics, Structures, Components, and Sub-Systems, SPIE Optical Engineering and Applications, San Diego, CA, USA, 25–29 August 2013. [\[CrossRef\]](#)
- Galehdar, A.; Nicholson, K.J.; Callus, P.J.; Rowe, W.S.T.; John, S.; Wang, C.H.; Ghorbani, K. The strong diamagnetic behaviour of unidirectional carbon fiber reinforced polymer laminates. *J. Appl. Phys.* **2012**, *112*, 113921. [\[CrossRef\]](#)
- Wang, W.X.; Takao, Y.; Matsubara, T. Galvanic Corrosion-Resistant Carbon Fiber Metal Laminates. In Proceedings of the 16th International Conference on Composite Materials, ICCM-16—“A Giant Step Towards Environmental Awareness: From Green Composites to Aerospace” (ICCM International Conferences on Composite Materials), Kyoto, Japan, 8–13 July 2007.
- Pimenta, S.; Pinho, S.T. Recycling carbon fibre reinforced polymers for structural applications: Technology review and market outlook. *Waste. Manag.* **2011**, *31*, 378–392. [\[CrossRef\]](#) [\[PubMed\]](#)
- Savage, G.; Oxley, M. Damage Evaluation and Repair of Composite Structures. *An. Mecánica Fract.* **2008**, *25*, 758–768.
- Heuer, H.; Schulze, M.; Pooch, M.; Gäbler, S.; Nocke, A.; Bardl, G.; Cherif, C.; Klein, M.; Kupke, R.; Vetter, R.; et al. Review on quality assurance along the CFRP value chain—Non-destructive testing of fabrics, preforms and CFRP by HF radio wave techniques. *Compos. Part B Eng.* **2015**, *77*, 494–501. [\[CrossRef\]](#)
- Das, S. Life cycle assessment of carbon fiber-reinforced polymer composites. *Int. J. Life Cycle Assess.* **2011**, *16*, 268–282. [\[CrossRef\]](#)
- La Magna, R.; Waimer, F.; Knippers, J. Coreless Winding and Assembled Core—Novel fabrication approaches for FRP based components in building construction. *Constr. Build. Mater.* **2016**, *127*, 1009–1016. [\[CrossRef\]](#)
- Minsch, N.; Müller, M.; Gereke, T.; Nocke, A.; Cherif, C. 3D truss structures with coreless 3D filament winding technology. *J. Compos. Mater.* **2019**, *53*, 2077–2089. [\[CrossRef\]](#)
- Büchler, D.; Elsken, T.; Glück, N.; Sier, M.; Bludszweit, S. Ultraleichte Raumzelle—Entwicklung von ultraleichten Großstrukturen in Faserverbund- und Hybridbauweise für den Schiffbau. In *Statusagung Schifffahrt und Meerestechnik*, 1st ed.; Forschungszentrum: Jülich, Germany, 2011; pp. 25–45.
- Prado, M. Skeletal composites: Robotic fabrication processes for lightweight multi-nodal structural components. *Constr. Robot.* **2020**, *4*, 217–226. [\[CrossRef\]](#)
- Duque Estrada, R.; Kannenberg, F.; Wagner, H.J.; Yablonina, M.; Menges, A. Spatial winding: Cooperative heterogeneous multi-robot system for fibrous structures. *Constr. Robot.* **2020**, *4*, 205–215. [\[CrossRef\]](#)
- Hunt, C.J.; Morabito, R.; Grace, C.; Zhao, Y.; Woods, B.K.S. A review of composite lattice structures. *Compos. Struct.* **2022**, *284*, 115120. [\[CrossRef\]](#)
- Dambrosio, N.; Zechmeister, C.; Bodea, S.; Koslowski, V.; Gil Pérez, M.; Rongen, B.; Knippers, J.; Menges, A. Towards an architectural application of novel fiber composite building systems—The BUGA Fibre Pavilion. In Proceedings of the 39th Annual Conference of the Association for Computer Aided Design in Architecture, Austin, TX, USA, 24–26 October 2019; ACADIA: Fargo, ND, USA, 2019; pp. 140–149.

16. Bodea, S.; Dambrosio, N.; Zechmeister, C.; Gil Pérez, M.; Koslowski, V.; Rongen, B.; Dörstelmann, M.; Knippers, J.; Menges, A.; Kyjaneck, O. BUGA Fibre Pavilion: Towards robotically-fabricated composite building structures. In *Fabricate 2020*; Burry, J., Sabin, J.E., Sheil, B., Skavara, M., Eds.; UCL Press: London, UK, 2020; pp. 234–243.
17. Polini, W.; Sorrentino, L. Influence of winding speed and winding trajectory on tension in robotized filament winding of full section parts. *Compos. Sci. Technol.* **2005**, *65*, 1574–1581. [[CrossRef](#)]
18. Arrabiyeh, P.A.; May, D.; Eckrich, M.; Dlugaj, A.M. An overview on current manufacturing technologies: Processing continuous rovings impregnated with thermoset resin. *Polym. Compos.* **2021**, *42*, 5630–5655. [[CrossRef](#)]
19. Mindermann, P.; Bodea, S.; Menges, A.; Gresser, G.T. Development of an Impregnation End-Effector with Fiber Tension Monitoring for Robotic Coreless Filament Winding. *Processes* **2021**, *9*, 806. [[CrossRef](#)]
20. Gil Pérez, M.; Zechmeister, C.; Kannenberg, F.; Mindermann, P.; Balangé, L.; Guo, Y.; Hügle, S.; Gienger, A.; Forster, D.; Bischoff, M.; et al. Computational co-design framework for coreless wound fibre-polymer composite structures. *J. Comput. Des. Eng.* **2022**, in press.
21. Quanjin, M.; Rejab, M.R.M.; Idris, M.S.; Kumar, N.M.; Merzuki, M.N.M. Robotic Filament Winding Technique (RFWT) in Industrial Application: A Review of State of the Art and Future Perspectives. *Int. Res. J. Eng. Technol.* **2018**, *5*, 1668–1676.
22. Munro, M. Review of Manufacturing of Fiber Composite Components by Filament Winding. *Polym. Compos.* **1988**, *9*, 352–359. [[CrossRef](#)]
23. Vasiliev, V.V.; Barynin, V.A.; Razin, A.F. Anisogrid composite lattice structures—Development and aerospace applications. *Compos. Struct.* **2012**, *94*, 1117–1127. [[CrossRef](#)]
24. Sorrentino, L.; Anamateros, E.; Bellini, C.; Carrino, L.; Corcione, G.; Leone, A.; Paris, G. Robotic filament winding: An innovative technology to manufacture complex shape structural parts. *Compos. Struct.* **2019**, *220*, 699–707. [[CrossRef](#)]
25. Bodea, S.; Zechmeister, C.; Dambrosio, N.; Dörstelmann, M.; Menges, A. Robotic coreless filament winding for hyperboloid tubular composite components in construction. *Automat. Constr.* **2021**, *126*, 103649. [[CrossRef](#)]
26. Gil Pérez, M.; Rongen, B.; Koslowski, V.; Knippers, J. Structural Design, Optimization and Detailing of the BUGA Fibre Pavilion. *Int. J. Space Struct.* **2020**, *35*, 147–159. [[CrossRef](#)]
27. Rongen, B.; Koslowski, V.; Gil Pérez, M.; Knippers, J. Structural optimisation and rationalisation of the BUGA fibre composite dome. In Proceedings of the IASS Annual Symposium—Structural Membranes—Form and Force, Barcelona, Spain, 7–10 October 2019.
28. Bodea, S.; Mindermann, P.; Gresser, G.T.; Menges, A. Additive Manufacturing of Large Coreless Filament Wound Composite Elements for Building Construction. *3d Print. Addit. Manuf.* **2021**. [[CrossRef](#)]
29. Gil Pérez, M.; Früh, N.; La Magna, R.; Knippers, J. Integrative structural design of a timber-fibre hybrid building system fabricated through coreless filament winding: Maison Fibre. *J. Build. Eng.* **2022**, *49*, 104114. [[CrossRef](#)]
30. Mindermann, P.; Rongen, B.; Gubetini, D.; Knippers, J.; Gresser, G.T. Material Monitoring of a Composite Dome Pavilion Made by Robotic Coreless Filament Winding. *Materials* **2021**, *14*, 5509. [[CrossRef](#)] [[PubMed](#)]
31. De Lima, A.S.; De Faria, A.R.; Faria, J.J.R. Critical Review of Displacement-Based Laminate Theories and Modeling Techniques. In Proceedings of the 4th Brazilian Conference on Composite Materials, Rio de Janeiro, Brazil, 22–25 July 2018. [[CrossRef](#)]
32. Menges, A.; Knippers, J.; Wagner, H.J.; Zechmeister, C. Pilotprojekte für ein Integratives Computerbasiertes Planen und Bauen. In *Baustatik–Baupraxis*, 14th ed.; Bischoff, M., Scheven, M., Bastian, O., Eds.; University of Stuttgart: Stuttgart, Germany, 2020; pp. 67–79.
33. Mindermann, P.; Gresser, G.T. Robotic 3D Deposition of Impregnated Carbon Rovings with Gradient Properties for Primary Structures. In Proceedings of the 69th International Astronautical Congress, Bremen, Germany, 1–5 October 2015.
34. Cayley, A. A theorem on trees. *Quart. J. Math.* **1889**, *23*, 376–378.
35. Dreißig, D.; Faßbänder, P.; Hindenlang, U. Simulation of carbon-roving-structures-extreme light and strong by filament wound reinforcement. In Proceedings of the 6th BETA CAE International Conference, Thessaloniki, Greece, 10–12 June 2015.
36. Gil Pérez, M.; Rongen, B.; Koslowski, V.; Knippers, J. Structural design assisted by testing for modular coreless filament-wound composites: The BUGA Fibre Pavilion. *Constr. Build Mater.* **2021**, *301*, 124303. [[CrossRef](#)]
37. Prashanth, S.; Subbaya, K.M.; Nithin, K.; Sachhidananda, S. Fiber Reinforced Composites—A review. *J. Mater. Sci. Eng.* **2017**, *6*, 1000341. [[CrossRef](#)]
38. Hitzler, L.; Merkel, M.; Hall, W.; Öchsner, A. A Review of Metal Fabricated with Laser- and Powder-Bed Based Additive Manufacturing Techniques: Process, Nomenclature, Materials, Achievable Properties, and its Utilization in the Medical Sector. *Adv. Eng. Mater.* **2018**, *20*, 1700658. [[CrossRef](#)]
39. Früh, N.; Knippers, J. Multi-stage filament winding: Integrative design and fabrication method for fibre-reinforced composite components of complex geometries. *Compos. Struct.* **2021**, *268*, 113969. [[CrossRef](#)]
40. Shai, O.; Preiss, K. Graph theory representations of engineering systems and their embedded knowledge. *Artif. Intell. Eng.* **1999**, *13*, 273–285. [[CrossRef](#)]
41. Wang, J.; Lu, M.; Belardo, F.; Randić, M. The anti-adjacency matrix of a graph: Eccentricity matrix. *Discret. Appl. Math.* **2018**, *251*, 299–309. [[CrossRef](#)]
42. Zechmeister, C.; Bodea, S.; Dambrosio, N.; Menges, A. Design for long-span coreless wound, structural composite building elements. In *Impact: Design with All Senses*; Gengnagel, C., Baverel, O., Burry, J., Ramsgaard-Thomsen, M., Weinzierl, S., Eds.; Springer: Berlin, Germany, 2020; pp. 401–415.

43. Mindermann, P.; Gil Pérez, M.; Kamimura, N.; Knippers, J.; Gresser, G.T. Implementation of Fiber-Optical Sensors into Coreless Filament-Wound Composite Structures. 2022, *submitted*.
44. Mindermann, P.; Gresser, G.T. Adaptive Winding Pin and Hooking Capacity Model for Coreless Filament Winding. 2022, *submitted*.
45. Harris, C.R.; Millman, K.J.; Van der Walt, S.J.; Gommers, R.; Virtanen, P.; Cournapeau, D.; Wieser, E.; Taylor, J.; Berg, S.; Smith, N.J.; et al. Array programming with NumPy. *Nature* **2020**, *585*, 357–362. [[CrossRef](#)] [[PubMed](#)]
46. McKinney, W. Data Structures for Statistical Computing in Python. In Proceedings of the 9th Python in Science Conference (SciPy 2010), Austin, TX, USA, 28 June–3 July 2010.
47. Plotly Technologies Inc. *Collaborative Data Science*; Plotly Technologies Inc.: Montréal, QC, Canada, 2015. Available online: <https://plot.ly>. (accessed on 4 February 2022).
48. Virtanen, P.; Gommers, R.; Oliphant, T.E.; Haberland, M.; Reddy, T.; Cournapeau, D.; Burovski, E.; Peterson, P.; Weckesser, W.; Bright, J.; et al. SciPy 1.0: Fundamental algorithms for scientific computing in Python. *Nat. Methods* **2020**, *17*, 261–272. [[CrossRef](#)] [[PubMed](#)]
49. DIN 16459:2021-06—Determination of the Fiber Volume Content of Fiber-Reinforced Plastics by Thermogravimetric Analysis (TGA). Available online: <https://www.beuth.de/en/standard/din-16459/336402982> (accessed on 4 February 2022).
50. Dempe, S. Eulersche Graphen und das Problem des chinesischen Postboten. In *Springer-Taschenbuch der Mathematik—Begründet von I.N. Bronstein und K.A. Semendjaew*, 3rd ed.; Zeidler, E., Grosche, G., Ziegler, V., Ziegler, D., Eds.; Springer: Wiesbaden, Germany, 2013; pp. 1070–1071.
51. SLM Solutions—Robust Selective Laser Melting—Multiple Lasers and Process Stability for Demanding Applications—SLM 280 Selective Laser Melting Machine. Available online: https://www.slm-solutions.com/fileadmin/Content/Machines/SLM_R_280_Web.pdf (accessed on 4 February 2022).
52. IPG Photonics Corporation—YLR-1070 Series—Ytterbium Fiber Lasers (Model YLR-400WC). Available online: <https://www.ipgphotonics.com/de/172/FileAttachment/YLR-1070+Series+Datashet.pdf> (accessed on 4 February 2022).
53. Zeiss Metrotom 1500. Available online: https://asset-downloads.zeiss.com/catalogs/download/iqs/ed81f139-455f-478c-bef0-2dc41802fa18/ZEISS_METROTOM_1500_Flyer_EN.pdf (accessed on 4 February 2022).
54. Mindermann, P.; Witt, M.U.; Gresser, G.T. Pultrusion-winding: A novel fabrication method for coreless wound fiber-reinforced thermoset composites with distinct cross-section. *Compos. Part A Appl. Sci. Manuf.* **2022**, *154*, 106763. [[CrossRef](#)]
55. Yang, W.; Lin, J.; Gao, N.; Yan, R. Experimental Study on the Static Behavior of Reinforced Warren Circular Hollow Section (CHS) Tubular Trusses. *Appl. Sci.* **2018**, *8*, 2237. [[CrossRef](#)]
56. Teijin Tenax Filament Yarn—Product Data Sheet (EU). Available online: https://www.teijincarbon.com/fileadmin/PDF/Datenblätter_en/Product_Data_Sheet_TSG01en_EU_Filament_.pdf (accessed on 4 February 2022).
57. Hexion—Epoxy Hand Lay-up Systems for Wind Blades (EPIKOTE Resin MGS LR 635 with LH 634–637). Available online: <https://www.hexion.com/en-us/applications/composites/wind/hand-lay-up> (accessed on 4 February 2022).